Global Dust Optical Depth Climatology Derived from CALIOP and MODIS Aerosol Retrievals on Decadal Time Scales: Regional and Interannual Variability

5   Qianqian Song[1,2], Zhibo Zhang[1,2,*], Hongbin Yu[3], Paul Ginoux[4], Jerry Shen[3,#]

1. Physics Department, UMBC, Baltimore, Maryland, USA
2. Joint Center of Earth Systems Technology, UMBC, Baltimore, Maryland, USA
10 3. Earth Sciences Division, NASA Goddard Space Flight Center, Greenbelt, Maryland, USA
4. NOAA Geophysical Fluid Dynamics Laboratory, Princeton, New Jersey, USA.

*Correspondence to: Zhibo Zhang, Zhibo.Zhang@umbc.edu
A summer intern worked at NASA Goddard Space Flight Center during June–August 2020.

Abstract

20   We present a satellite-derived global dust climatological record over the last two decades, including the monthly mean visible dust optical depth (DAOD) and vertical distribution of dust extinction coefficient at a 2° (latitude) × 5° (longitude) spatial resolution derived from CALIOP and MODIS. Dust is distinguished from non-dust aerosols based on particle shape

25   information (e.g., lidar depolarization ratio) for CALIOP, and on dust size and absorption information (e.g., fine-mode fraction, Angstrom exponent, and single-scattering albedo) for MODIS, respectively. On multi-year average basis, the global (60°S-60°N) and annual mean DAOD is 0.029 and 0.063 derived from CALIOP and MODIS retrievals, respectively. In most dust active regions, CALIOP DAOD generally correlates well with the MODIS DAOD, with

30   CALIOP DAOD being significantly smaller. CALIOP DAOD is 18%, 34%, 54% and 31% smaller than MODIS DAOD over Sahara Deserts, the tropical Atlantic Ocean, the Caribbean Sea, and the Arabian Sea, respectively. Over East Asia and the northwestern Pacific Ocean (NWP), however, the two datasets show weak correlation. Despite these discrepancies, CALIOP and MODIS show similar seasonal and interannual variations in regional DAOD. For dust aerosol

35   over NWP, both CALIOP and MODIS show a declining trend of DAOD at a rate of about 2% yr^{-1}. This decreasing trend is consistent with the observed declining trend of DAOD in the southern Gobi Desert at a rate of –3% yr^{-1} and –5% yr^{-1} according to CALIOP and MODIS, respectively. The decreasing trend of DAOD in the southern Gobi Desert is in turn found to be significantly correlated with an increasing trend of vegetation and a decreasing trend of surface

40   wind speed in the area.

1   Introduction

Mineral dust, referred to as dust for short, is one of the most abundant type of atmospheric aerosol in terms of dry mass (Textor et al. 2006; Yu et al. 2012; Kok et al. 2017). Dust aerosol directly interacts with both solar and thermal infrared radiation, known as the direct radiative effect, and thereby influences the Earth's radiative energy budget (Kok et al, 2017; Song et al., 2018; Di Biagio et al. 2020). Dust also influences the life cycle and properties of clouds by altering the thermal structure of the atmosphere (known as semi-direct effects) (Hansen et al., 1997) and by acting as cloud condensation nuclei (CCN) and ice nuclei (IN) (known as indirect effects) (Albrecht 1989; Rosenfeld and Lensky 1998; Twomey 1977). Dust storms and plumes can degrade air quality and generate adverse impacts on human health (Griffin, 2007; Querol et al., 2019). Dust also contains a variety of nutrients and the deposition of dust during transport provides essential nutrients to marine and terrestrial ecosystems (Jickells et al. 2005; Yu et al., 2015b). The deposition of dust on snow reduces the snow albedo and promotes snow melting (Painter et al., 2007). All these impacts manifest the important role of mineral dust in the Earth systems (e.g. Evan et al., 2006; Lau & Kim, 2007; Miller & Tegen, 1998; Shao et al., 2011)

Dust production is sporadic in nature and it can be transported on intercontinental, hemispherical, and even global scales (Grousset et al. 2003; Uno et al. 2009; Yu et al. 2012, 2013). Thus, global and routine measurements of dust spanning over years or even decades are vital for studying dust transport and deposition, estimating the dust radiative effects, and evaluating and constraining dust simulations in numerical weather and climate models. Satellite remote sensing is the only means to observe dust on regional to global scales. Satellite remote sensing techniques usually retrieve the optical depth or extinction profile for total aerosol in the

atmosphere with additional retrievals of particle size, shape, or absorption properties that are
sensor specific. Passive sensors, such as the Total Ozone Mapping Spectrometer (TOMS)
(Prospero et al., 2002), Ozone Monitoring Instrument (OMI) (Chimot et al. 2017), Multiangle
Imaging SpectroRadiometer (MISR) (Ge et al., 2014 and Y. Yu et al. 2019), Moderate
Resolution Imaging Spectroradiometer (MODIS) (Ginoux et al., 2010; Remer et al.,2005; Yu et
al., 2009), multi-angular and polarimetric POLDER/PARASOL measurements (Chen et al. 2018)
and IASI (Klüser et al., 2011; Clarisse et al. 2019) are used to detect dust sources and track dust
plumes at global scales. On one hand, these passive sensors provide global or quasi global
coverage of column integrated properties of aerosol with satisfactory temporal resolution. On the
other hand, they do not provide the vertical structure of aerosol that is critical for studying
aerosol-cloud interactions and aerosol influences on the thermal structure of the atmosphere.
Space-borne lidar systems, such as the Cloud-Aerosol Lidar with Orthogonal Polarization
(CALIOP) onboard the Cloud-Aerosol Lidar and Infrared Pathfinder Satellite Observation
(CALIPSO) spacecraft (Winker et al., 2010) and the Cloud-Aerosol Transport System (CATS)
onboard the International Space Station (Yorks et al. 2015) are able to provide the vertical
structure of aerosol and clouds, albeit with limited spatial coverage. All these passive and active
remote sensing observations have been used extensively in studies of the spatial and temporal
evolution of aerosol over the past decade (e.g., Proestakis et al. 2018).

A significant hurdle of applying satellite remote sensing measurements for dust studies is
how to distinguish dust from other aerosol types in a quantitative way. While many studies have
used total aerosol retrievals by focusing on regions and seasons where dust dominates, some
studies have developed sensor-specific methods of partitioning total aerosol into dust and non-

dust components with varying assumptions (Kaufman et al., 2005; Kalashnikova et al. 2005; Dubovik et al. 2006; Ginoux et al., 2010; Yu et al., 2009, 2013, 2015a, 2019). In general, the dust separation methods are based on dust physical and optical properties such as their large size,

90   their irregular or nonspherical shape, and absorption characteristics. For example, CALIOP dust classification is mainly based on the fact that dust aerosols are nonspherical in shape and their lidar depolarization ratio is significantly larger than those spherical aerosols. In contrast, the wide spectral coverage of MODIS measurements enables the retrieval of aerosol particle size information, such as effective radius, fine-mode fraction (FMF), and aerosol extinction

95   Angstrom exponent, as well as spectral gradient of absorption (decreasing of absorption from UV to red) (Remer et al., 2005). The combinations of these retrievals provide the basis for dust separation and DAOD retrievals from MODIS. Some recent studies have also characterized dust distribution through integrating satellite measurements with other data sources and model simulations. For example, Voss and Evan (2020) developed a dust optical depth record from

100   MODIS retrievals, similar to Kaufman et al. (2005) over ocean and Ginoux et al. (2012) over land. Unlike Kaufman et al. (2005) and Yu et al. (2020) that derived characteristic FMF values for combustion, dust, and marine aerosol from MODIS retrievals, Voss and Evan (2020) determined these characteristic FMFs from AERONET measurements. Voss and Evan (2020) also extended the MODIS-based method to AVHRR over-ocean retrievals with some

105   assumptions and produced the long-term (1981-2018) record of dust optical depth. Gkikas et al. (2020) developed a global fine resolution (0.1º x 0.1º) DAOD dataset for the period 2006-2017 by scaling MODIS retrieved AOD with the DAOD-to-AOD ratios provided by MERRA-2 (Modern-Era Retrospective analysis for Research and Applications, Version 2) reanalysis (Gelaro et al., 2017). Given that MODIS and other remote sensing measurements (e.g., MISR

110   and AERONET) have been assimilated in the MERRA-2 reanalysis to constrain the aerosol

optical depth, the DAOD-to-AOD ratio reported by MERRA-2 is the same as that from the

underlying GOCART aerosol transport model in the MERRA-2 reanalysis system.

    In this study, we focus on the dust optical depth derived from CALIOP and MODIS with two

115   major objectives. First, we produce a decadal (2007-2019) record of global DAOD and dust

vertical extinction coefficient profile climatology from the CALIOP observations, which

represents an extension of the trans-Atlantic dust transport and deposition studies by Yu et al.

(2015a, 2015b, 2019), both in terms of spatial and temporal coverages. Second, we compare the

CALIOP DAOD climatology with the MODIS DAOD over both land and ocean (Yu et al. 2020;

120   Pu and Ginoux, 2018) to identify and understand their differences in terms of global dust

distribution and interannual variabilities including decadal trend in key dust regions. Our

analysis goes beyond broad dust-laden regions by zooming into potential dust source areas,

which provides important insights into local dust activities. A systematic comparison and better

understanding of DAOD from the two sensors based on distinct retrieval algorithms is critical for

125   applying satellite measurements to evaluate global dust modeling (Kim et al. 2019). In

comparison to some most recent studies (Voss and Evan, 2020; Gkikas et al. , 2020), our dust

climatology is derived by using the satellite observations in a self-consistent way without

blending in other measurements (e.g., AERONET) or models (e.g., MERRA-2) (see section 2 for

details). As discussed in Yu et al. (2009), the self-consistent use of MODIS data could minimize

130   the introduction of additional biases due to discrepancies in FMF between MODIS and

AERONET. Furthermore, we use the latest version 4.2 CALIOP products and version 6.1

MODIS products in this study to characterize the three-dimensional distributions of dust. The

rest of the paper is organized as follows. Section 2 provides a description of the methodology of deriving dust climatology from CALIOP and an overview of MODIS dust retrieval algorithm. Section 3 provides the main results including analysis of CALIOP dust climatology data and its comparison against MODIS dust data. Section 4 discusses the uncertainties in CALIOP as well as MODIS DAOD retrievals. Section 5 provides a summary of the study along with the main conclusions.

2 Dust Detection and AOD Partition Schemes

2.1   CALIOP Dust Detection and AOD Partition

CALIPSO is in a sun-synchronous polar orbit with an equator crossing time of around 13:30 local time and 98° orbit inclination. CALIOP is a two-wavelength (532nm and 1064nm) polarization-sensitive lidar onboard CALIPSO. CALIPSO orbit track repeats every 16 days, CALIOP sensor never provides global coverage due to its small footprint. At Earth's surface, the diameter of CALIOP footprint is around 70m, with spacing distance of 333m between two adjacent footprints along the orbit track. CALIOP utilizes three receiver channels (one measuring the 1064nm backscatter intensity and two measuring orthogonally polarized components of the 532nm backscatter) to provide high vertical resolution 30-60m of aerosol and cloud structure profiles (Winker et al., 2009).

Aerosol subtype classification and a priori assumption of lidar ratio for specific aerosol type are critical for CALIOP aerosol retrievals. CALIOP Level 2 product has been validated by comparing with ground-based measurements. The comparison between aerosol subtypes in CALIOP level 2 V2.01 and NASA Aerosol Robotic Network (AERONET) aerosol types shows that 70% of the CALIOP and AERONET aerosol types are in agreement. Best agreement is

achieved for dust and polluted dust (Mielonen et al. 2009). Schuster et al. (2012) compared CALIOP AOD to the collocated AERONET AOD measurements and found a CALIPSO bias of −13%, corresponding to an absolute bias of −0.029 relative to AERONET AOD on global average. Further comparison between CALIPSO AOD measurements and the collocated

160   AERONET AOD measurements for the columns that contain the dust subtype exclusively showed a larger bias (i.e., −29% and corresponding absolute bias of −0.1), although they show a relatively high correlation of R=0.58; this indicates that the assumed lidar ratio (40 sr) for the CALIPSO dust retrievals is too low. Omar et al. 2013 showed that CALIOP AOD are lower than AERONET AOD especially for low AOD. Furthermore, they found that the median of relative

165   AOD difference between CALIOP and AERONET (500nm) is 25% of AERONET AOD for AOD > 0.1.

CALIOP observations have been used widely in previous studies of the spatial and temporal evolution of dust aerosols over the past decade (Huang et al. 2007, 2008; Yang et al. 2012; Xu et al. 2016; Kim et al., 2019). It is important to note that these studies are regional in scope and

170   they use the standard CALIPSO product and aerosol subtype classification algorithm (Omar et al. 2009). In the standard CALIPSO product, each detected aerosol layer is classified as one of the six subtypes: dust, polluted dust, polluted continental, smoke, clean marine and clean continental. In the latest CALIOP version, another sub-type "marine-dust" is introduced (Kim et al. 2018). In these studies, the "dust" subtype or a combination of "dust" and "polluted dust" subtypes is

175   categorized as dust. While the former assumption leads to an underestimate of dust due to neglecting dust component in the "polluted-dust" subtype, the latter assumption results in an overestimate of dust because of accounting for non-dust component in the "polluted-dust" subtype. In order to better distinguish dust component from each CALIOP detected aerosol

layers, Yu et al. (2015a) developed an algorithm independent of the standard aerosol subtype

180   classification to distinguish dust from non-dust aerosol by using their respective thresholds of

particulate depolarization ratio. They further used the derived three-dimensional distribution of

dust extinction to quantify the trans-Atlantic dust transport and deposition and its implications

for Amazon rainforest (Yu et al., 2015b, 2019).

185   In this study, we use the methodology in Yu et al. (2015a) to derive the monthly mean dust

extinction profile under clear-sky conditions from the latest V4.20 CALIOP products on a global

scale from 2007 to 2019. First, we select the clear-sky profiles based on the operational CALIOP

vertical feature mask and cloud layer product. In order to increase the sampling, we define clear-

sky cases in this study either as columns that are completely cloud-free or with the presence of

190   optically thin (cloud optical depth < 0.2) and high-level (cloud base > 7km) clouds. This is

justified that the presence of high-level optically thin clouds does not significantly affect the

retrieval of aerosol layers below the clouds (Yu et al. 2015a). After clear-sky screening, we use

the operational 5 km level 2 CALIOP aerosol profile product that contains aerosol

depolarization, backscatter and extinction profiles over a global scale (Young et al. 2018) to

195   derive the dust extinction profile. The depolarization ratio from CALIOP is a key variable for

detecting and distinguishing dust from non-dust aerosol. Backscatter by spherical particle largely

retains the polarization of the incident light, resulting in a depolarization ratio of nearly zero. In

contrast, dust particles are generally non-spherical in shape and large in size, which gives them

non-zero depolarization ratio that is significantly larger than other types of aerosol. The cloud-

200   aerosol discrimination (CAD) score in the products gauges the level of confidence for a feature

being classified as aerosol or cloud. In this study, in order to screen out low-confidence aerosol

and cloud discrimination, we select layers with CAD scores between −90 and −100 (high level of confidence for aerosol feature) by following Yu et al. (2019). Aerosol profile product also provides extinction quality control flag (Ext_QC) to indicate problematic retrievals. This study

205   only uses layers with Ext_QC values of 0, 1, 18, and 16 (Winker et al., 2013). Only nighttime data are used to avoid sunlight interference in aerosol signals.

For each backscatter coefficient profile, we derive the fraction of dust backscatter to total backscatter (f_d) at each altitude from the following equation

$$f_d = \frac{(\delta - \delta_{nd})(1 + \delta_d)}{(\delta_d - \delta_{nd})(1 + \delta)} \, , \tag{1}$$

where δ is CALIOP observed particulate depolarization ratio, δ_d and δ_{nd} is a priori knowledge

210   of depolarization ratios of dust and non-dust aerosols respectively. Clearly, the calculations of f_d in Eq. (*1*) rely on the a priori depolarization ratios of dust and non-dust aerosols (i.e., δ_d and δ_{nd}). To account for various types of non-dust aerosols with different depolarization ratio, we follow Yu et al. 2015a and assume 0.02 and 0.07 as lower and upper bounds for δ_{nd} (Burton et al., 2012; Fiebig et al., 2002; Sakai et al., 2010). Dust aerosols have significantly larger

215   depolarization ratio compared to non-dust aerosols. In order to account for the variability of dust shape and size, we use 0.2 and 0.3 as lower and upper bounds for δ_d (Ansmann et al., 2012; Esselborn et al., 2009; Sakai et al., 2010). Given an observed dust depolarization ratio δ, the f_d based on Eq. (*1*) has the minimum value when $\delta_d = 0.30$ and $\delta_{nd} = 0.07$ and the maximum value when $\delta_d = 0.20$ and $\delta_{nd} = 0.02$. In order to account for this variability, the final f_d is

220   based on the mean of the lowest (i.e., $\delta_d = 0.30$ and $\delta_{nd} = 0.07$) and the highest (i.e., $\delta_d = 0.20$ and $\delta_{nd} = 0.02$) dust scenario. The DAOD is also calculated for low dust and high dust scenarios for uncertainty study in section 4.

Dust backscatter coefficient profiles are derived by multiplying CALIOP total backscatter

225 coefficient with the calculated f_d from Eq. 1. In order to derive dust extinction coefficient from

dust backscatter coefficient, we assume dust lidar ratio (LR), i.e., extinction to backscatter ratio,

of 44 sr at 532nm, consistent with CALIOP Version 4.20 operational retrieval (Kim et al., 2018).

The use of globally uniform LR could also induce uncertainty to the derived regional DAOD,

which is discussed in section 4.

230

2.2 MODIS Dust Detection and AOD Partition

As described above, the CALIOP-based DAOD derivation mainly makes use of dust non-

sphericity in shape to separate dust aerosol from others. Another important difference of dust

aerosol from other types of aerosols is their relatively large size. This difference provides the

235 basis for the dust separation and DAOD derivation scheme based on the Moderate Resolution

Imaging Spectroradiometer (MODIS) retrievals that is introduced in this section.

MODIS sensors onboard of the Aqua and Terra satellites measure radiances at 36 spectral

bands ranging from 0.41 to 14 μm, with a 2330 km swath that provides near-global coverage

240 every day. As aforementioned, we use CALIOP nighttime observations to avoid solar

contamination. However, MODIS AOD retrievals rely on the solar reflective bands and therefore

are only available during daytime. Kittaka et al., 2011 shows that daytime and nighttime global

seasonal-mean AOD distributions for JJA 2006 from CALIOP are generally similar in both

outflow and source regions (see their Figure 1). It is difficult to tell what caused the minor

245 differences because it could be a combination of different calibration procedures and algorithms

for day and for night, different spatial sampling, and diurnal changes in the aerosol. Based on

this consideration, we choose to use the nighttime CALIOP product that is free of solar noise, in hoping that the better data quality would outweigh the diurnal difference between nighttime CALIOP product and daytime MODIS retrievals.

250

MODIS aerosol retrievals employ two complementary algorithms to achieve the global coverage. The Dark Target (DT) algorithm is applicable for the retrieval of aerosol loading and properties over dark surfaces, including ocean-water and vegetated land. The MODIS aerosol AOD retrievals over ocean are found within the retrieval errors of $\Delta\tau_a = \pm 0.03 \pm 0.05\tau_a$

255 relative to AERONET AOD measurements (Remer et al. 2005). An approach was developed in previous studies to separate DAOD from other types of aerosol by using aerosol optical depth τ and fine mode fraction retrieved from MODIS DT retrieval over ocean (details can be found in Kaufman et al., 2005; Yu et al., 2009, 2020). Over land, MODIS aerosol properties including AOD, Angstrom exponent, SSA are retrieved from the Deep Blue (DB) algorithm (Hsu et al.

260 2004, 2013). The MODIS aerosol AOD retrievals over land are found within the retrieval errors of $\Delta\tau_a = \pm 0.05 \pm 0.15\tau_a$ relative to AERONET AOD measurements (Remer et al. 2005). To separate dust from scattering aerosols, it is required that the single-scattering albedo at 470nm to be less than 0.99. Then a continuous function relating the Angstrom exponent to fine-mode AOD is used to separate dust from fine particles (more details can be found in Pu and Ginoux, 2018).

265 Overall, multi-wavelength observations from MODIS contains aerosol size information such as fine-mode fraction and Angstrom exponent in the observed reflectance spectral pattern, which was used to separate dust aerosol from others in MODIS dust retrieval over ocean and land. In this study, the latest retrieved aerosol properties from MODIS Collection 6.1 are used. We use data from Aqua MODIS only, because Terra MODIS retrievals may generate spurious dust trend

270   (Yu et al. 2020). In order to minimize cloud contamination and avoid the infrequent sampling to

bias DAOD in MODIS dust retrieval over ocean, we screen the data by requiring a minimum of

10 DAOD retrievals in a month.

3   Global Dust Climatology

Based on the dust detection and separation schemes of two sensors described above, we derived

275   the following two datasets:

1. The monthly mean CALIOP-based total aerosol optical depth (TAOD) and DAOD, as well
    as the vertical extinction profile on a 2º (latitude) ×5º (longitude) spatial resolution grids for
    the period of 2007 – 2019. This relatively coarse resolution is limited by CALIOP's sampling.

2. We combine the monthly mean Aqua MODIS over-ocean (Yu et al., 2020) and over-land (Pu

280   and Ginoux, 2018) TAOD and DAOD on a 1º ×1º spatial resolution grids to get the monthly
    mean MODIS-based TAOD and DAOD from 2003 to 2019. In order to compare with
    CALIOP-based dust climatology data, we aggregate the 1º ×1º MODIS-based data to 2º ×5º
    resolution grids.

3. For evaluation and comparison purpose (see section 3.1), we also produce a seasonal global

285   distribution of conditionally sampled DAOD from CALIOP. Different from the
    climatological DAOD introduced above, where we include all cloud-free cases in the average
    of dust extinction and DAOD regardless of the presence of dust or not. In other words,
    DAOD and dust extinction are assumed to be zero when no dust is detected. In the
    conditionally sampled DAOD calculation, we only average those cases where dust is

290   detected (i.e., DAOD and dust extinction are non-zero). Therefore, the conditionally sampled
    DAOD is directly related to the intensity of the detected dust events, whereas the
    climatological DAOD is determined by a number of factors including not only the intensity

of the detected dust events but also the frequency of the dust events as well as the capability

of the instrument to sample the dust events.

295

In this section, we compare shape-based CALIOP global dust retrieval against size-based

MODIS dust retrieval, more specifically MODIS ocean dust retrieval from Yu et al. (2009, 2020)

and land dust retrieval from Pu and Ginoux (2018), we analyze the similarities and differences

between two dust climatology data and furthermore study seasonal cycle and decadal trend of

300   dust aerosols based on these datasets.

3.1 Comparison between CALIOP and MODIS dust Climatology

The DAOD climatology datasets derived from the CALIOP and MODIS observations, as

described in the last section, have two major sources of uncertainty:

1) The uncertainty associated with the AOD retrieval. The primary uncertainty sources in

305   MODIS AOD retrieval include instrument calibration errors, cloud-masking errors, inappropriate

assumption of surface reflectance and aerosol model selection (Remer et al. 2005; Levy et al.

2013, 2018). Uncertainty sources in CALIOP aerosol retrieval include instrument calibration

errors, errors in discriminating cloud from aerosol, uncertainties associated with the a priori

assumption of lidar ratios, and the under detection of tenuous aerosol layers, and overestimation

310   of the elevation height of heavy aerosol plume base (Winker et al. 2009; Yu et al., 2010;

Schuster et al., 2012; Thorsen and Fu, 2015; Rajapakshe et al. 2017).

2) The uncertainty associated with dust detection and separation. As explained in section 2,

CALIOP- and MODIS-based dust detection and separation methods are based on different

characteristics of dust aerosols in comparison with other types of aerosols, as summarized in

315   Table 1. CALIOP-based method makes use of the fact that depolarization ratio of dust aerosols is

much higher than other types of aerosols, primarily because of irregular non-spherical shape and also to a lesser extent because of coarse size of dust particles. MODIS-based method is largely based on the characteristics of coarse particle size. Over ocean, DAOD is derived from total aerosol AOD (TAOD) and fine mode fraction (FMF) with a priori characteristic FMF for

320 individual aerosol types. Over land, DAOD is derived using spectral dependence of aerosol extinction (i.e., Angstrom exponent) and single scattering albedo. In other words, MODIS retrieves DAOD based on dust size supplemented by absorption characteristics.

Given these retrieval uncertainties and methodological differences, some discrepancies between the two DAOD climatology datasets are expected. In this section, we will compare the

325 two datasets to identify and understand their similarities and differences. Since the mechanisms of dust generation, dust transport and dust removal processes all have a seasonal cycle (Mbourou et al. 1997; Parrington et al. 1983), we first present and discuss dust spatial distributions for each season in this section. Table 2 summarizes the seasonal and annual mean DAOD and TAOD values averaged over ocean, land and the globe (all limited to 60° S-60° N), respectively, based

330 on MODIS and CALIOP dust retrievals from 2007 to 2019. On multi-year average basis, the global, annual mean DAOD (TAOD) is 0.029 (0.112) and 0.063 (0.167) according to CALIOP and MODIS retrieval, respectively. Generally, DAOD from two retrievals differ by a factor of about 3 over ocean and less than 2 over land, while TAOD differ by a factor of less than 2 over both ocean and land. The ratio of DAOD over land to that over ocean is about 2 and 3 for

335 MODIS and CALIOP, respectively. For TAOD, the land to ocean ratio is about 2 for both products. Overall, the difference in TAOD between two retrievals is less than their difference in DAOD. On a global average, both MODIS and CALIOP-based DAOD peaks in boreal summer (June-July-August). DAOD reaches minimum in boreal Fall (September-October-November) for

MODIS but in boreal Winter (December-January-February) for CALIOP. The MODIS and

340   CALIOP differences are region dependent, which is discussed as follows.

Figure 1 shows the spatial distribution of seasonal mean DAOD and the percentage of

DAOD to the TAOD based on 13-year (2007-2019) CALIOP and MODIS observations. Note

that this period is chosen because both datasets are available. Generally, MODIS-based DAOD is

larger than CALIOP-based DAOD. As expected, high values are seen from both CALIOP-based

345   and MODIS-based DAOD over the 'dust belt' regions extending from the west coast of North

Africa to the Middle East, Central Asia, and China, where large-scale dust activities occur

persistently throughout the year. However, the CALIOP-based DAOD is rather low in some

other regions that are known to be dusty in certain seasons, such as the southwestern United

States, South America (Patagonian Desert), Australia, and South Africa (i.e., Kalahari Desert).

350   These regions do stand out in MODIS DAOD maps (i.e., the second column in Figure 1).

Interestingly, these regions indeed show up in the DAOD to TAOD ratio plot based on both two

sensors (i.e., the last two columns in Figure 1). One of possible reasons for this is that dust

activities in those regions are more intermittent and CALIOP's narrow swath results in more

frequent miss of detection than MODIS does. To test this hypothesis, we compare the seasonal

355   climatological DAOD and conditional DAOD product. The second column of Figure 2 shows the

seasonal climatological DAOD which is the average dust load over a geographical domain and

time interval. It contains information of both the intensity and frequency of dust activities. On

the other hand, the seasonal conditionally sampled DAOD shown in the first column of Figure 2

eliminates the impacts from dust frequency by excluding dust-free cases in the average. It is

360   mainly related to the intensity of observed dust events. Therefore, the comparison between

climatological and conditionally sampled DAOD sheds a light on the frequency and intensity of

dust events. For example, the third column in Figure 2 shows the relative difference between conditionally sampled DAOD and climatological DAOD with respect to the climatological DAOD. In 'dust belt' regions, especially in Sahara Desert and Middle East where dust activities are persistent, climatological DAOD is very close to conditional DAOD. In Australia, Southwest United State, South America and South Africa, however, the conditional DAOD (column 1 in Figure 2) and the difference (column 3 in Figure 2) are relatively high. This suggests that dust activities in those regions are highly episodic and/or occur in relatively small scales. As a result, the dust events in those regions are prone to be missed by CALIOP due to its once-a-day sampling over limited spatial coverage. Even if the episodic dust events are sampled by CALIOP, the monthly averaging would diminish the sparse daily DAOD retrievals in those regions. Indeed, Prospero (1999) reported that dust signals were shown in the daily TOMS aerosol index (AI) product in those regions but were not captured in TOMS monthly-mean AI product. The difference also is very large in open oceans, suggesting that dust aerosols are present at a very low frequency.

Having analyzed the conditionally sampled DAOD from CALIOP, we now return to climatological DAOD and comparison between CALIOP and MODIS. Hereafter, all AOD values are climatological without otherwise explicit statement. Figure 3 shows the difference in seasonal mean TAOD, DAOD and the percentage of DAOD in TAOD between MODIS retrievals and CALIOP retrievals. We note in Figure 3 that CALIOP-based DAOD is generally smaller than MODIS-based DAOD over Northeast Asia and Asian dust outflow region (Northwest Pacific-NWP). There could be several reasons for this. First, this region is a major outflow region of Asian pollution (Yu et al., 2020). It is possible that the internal mixing of dust

385 aerosols with industrial pollution in this region changes the dust morphology making it less non-spherical (Li and Shao 2009) but larger in size, which leads to smaller depolarization ratio and smaller fine-mode fraction. As a result, CALIOP shape-based DAOD derivation method could not capture the dust particles contained in the mixture, while those dust particles can be captured by MODIS size-based method. Another potential reason could be associated with that dust

390 plumes in this region are vertically dispersed (Yu et al., 2010; Su and Toon, 2011). These tenuous dust layers are likely to go undetected by CALIOP because of its relatively low sensitivity. However, MODIS retrieves aerosol from the columnal integrated reflectance which is not dependent on the vertical distribution of aerosol.

  The difference may also be caused by uncertainties in MODIS aerosol retrievals. The

395 West Pacific Ocean is cloudy almost all year long (see the last column in Figure 3), which makes MODIS aerosol retrievals being susceptible to cloud contamination. The cloud contamination can lead to an overestimation of TAOD but underestimation of FMF. Although the MODIS retrieval algorithm neither assume coarse particles are exclusively from dust aerosols nor assume dust particles are all coarse particles (Yu et al., 2020), coarse mode aerosols are primarily dust.

400 Thus, the overestimation of TAOD and underestimation of FMF will lead to an overestimation in DAOD. An exception occurs during winter when cloud fraction is large in NWP. The MODIS-based DAOD is smaller than CALIOP-based DAOD, even though MODIS TAOD is larger than CALIOP TAOD. Similarly, over the southeastern Atlantic Ocean, CALIOP-based DAOD is also generally smaller than MODIS-based DAOD. On one hand, cloud contamination may have

405 biased the MODIS dust retrieval high. On the other hand, CALIOP clear-sky sampling is not large enough to capture some dust events in this region. In southern part of Sahel and India, MODIS-based DAOD is generally smaller than CALIOP-based DAOD.

We further compare DAOD (Figure 5) and TAOD (Figure S1 in the supplementary) retrievals from CALIOP and MODIS over major dust laden regions (as shown in Figure 4),

410   including three source regions on land (i.e., Sahara Desert, Middle East and Eastern Asia) and six oceanic outflow regions (i.e., the tropical Atlantic Ocean - TAT, the Caribbean Basin - CRB, the Mediterranean Sea - MED, the northwest Pacific Ocean - NWP, the Arabian Sea - ARB as well as the tropical Indian Ocean and the Bay of Bengal - IND). Each data point in the scatter plot represents a monthly mean DAOD (or TAOD) in a $2° \times 5°$ grid. The density of data is

415   represented by different color. To avoid our analysis being biased by some extreme and rare cases, we exclude those data points within the lowest 5% of data density (grey points in Figure 5). Overall, the DAOD from the two instruments correlate well ($R^2 > 0.5$) and on average CALIOP-based DAOD is 18%, 34%, 54% and 31% lower than MODIS-based DAOD over the Sahara (Figure 5a), TAT (Figure 5d), CRB(Figure 5e) and ARB(Figure 5h) regions, respectively. Over

420   the Sahara Desert, the good agreement in DAOD between the two sensors (bias of 18% and $R^2 =$ 0.61) suggests that over the Sahara Desert dust particles can be adequately characterized by both irregular non-spherical shape and coarse size. As a result, both CALIOP- and MODIS-based methods are able to detect and separate the dust from other types of aerosols. In TAT and ARB regions, two instruments correlate well ($R^2 > 0.7$) in both DAOD and TAOD. For TAOD,

425   CALIOP is smaller than MODIS by 2% in TAT and larger than MODIS by 15% in ARB. By comparison differences in DAOD are larger, with CALIOP DAOD lower than the MODIS DAOD by 34% and 31% in TAT and ARB, respectively. This suggests that the differences in DAOD from the two instruments are mainly resulted from differences in the dust separation method. In East Asia and NWP, on contrast, both TAOD and DAOD show poor correlation

430   between the two methods (Figure 5c, 5g, S1(c) and S1(g)). As discussed earlier, the poor

correlation between the two methods may be contributed by many factors. For example, the total TAOD retrievals from MODIS are subject to larger uncertainties due to cloud contamination, or the DAOD retrieval from CALIOP may miss spherical dust particles that are coated by large combustion emissions from East Asia.

435   Figure 6 compares annual cycle of MODIS and CALIOP DAOD based on the 13-year (2007-2019) average over the nine dust laden regions. Each data point represents domain-averaged 13-year mean DAOD for a month, while the error bar indicates $\pm 1\sigma$ (one standard deviation of DAOD). The seasonal cycles of dust activities and dust transport are consistent with results in literature (Prospero et al. 2002; Yu et al., 2012, 2015a). Generally, CALIOP and 440 MODIS show very similar seasonality over those dust laden regions. DAOD peaks in summer (JJA) over Sahara Desert, Middle East, TAT, CRB, ARB and IND, but in spring (MAM) over Eastern Asia, MED and NWP. Over NWP, the seasonal cycle of MODIS DAOD is somewhat different from that of CALIOP DAOD. While CALIOP DAOD peaks in spring, MODIS DAOD shows a peak in late spring or even summer months for some years. This could have resulted 445 from cloud contamination in MODIS retrievals due to the large cloud fraction in summer [Yu et al., 2020]. In addition, a secondary maximum of dust activity with high elevation plume in summer over the Taklamakan desert (Ginoux et al., 2001) may also contribute to the seasonality trend captured by MODIS over NWP.

       Compared to the MODIS dust retrieval, CALIOP has a unique capability of detecting 450 dust aerosol vertical distribution. Figure 7 shows seasonal mean dust extinction vertical profile from CALIOP for the nine dust-laden regions. The values on each plot represent the seasonal mean DAOD. Both DAOD and dust vertical structure have a seasonal dependence. In Sahara (a), Middle East (b) and their dust outflow regions the Tropical Atlantic (d) and the Arabian Sea (h),

summertime dust aerosol has the highest DAOD and reaches to the highest altitude extending

455   from surface up to 6km in altitude.

        The analysis above has been performed over the broad dust-laden regions. Here we focus

on MODIS and CALIOP comparison in major potential source areas (PSAs) for dust in North

Africa, namely NAF-1 to NAF-6 as illustrated in Figure 8 (adapted from Fig. 1 in Formenti et al.,

2011). Among all dust source regions around the globe, the Sahara Desert and its margins in

460   North Africa are the largest dust emitter. Within this region, prominent dust sources are often

associated with topographical lows and foothills of mountains (Prospero et al. 2002). Figure 9

shows scatterplots of CALIOP DAOD against MODIS DAOD over the six PSAs (corresponding

scatterplots for TAOD are shown in Figure S2 in the supplementary), with each data point

representing a monthly average over 2°×5° grid. Seasonal variations of DAOD in the six PSAs

465   are shown in Figure 10. Striking CALIOP and MODIS differences in both DAOD and TAOD

exist in NAF-5 where the correlation is very weak. NAF-5 (14N-20N, 15E-20E) is located in

Bodélé Depression, Western Chad. This region is reported as the most intense dust source in the

world (Prospero et al. 2002), and dust activity in the region occurs with a high frequency during

all seasons except fall (Mbourou et al., 1997). However, CALIOP TAOD and DAOD are much

470   smaller than MODIS retrievals in this region. In terms of dust seasonality (Figure 10), the

MODIS DAOD indicates intense dust aerosol loading all year long with a lower DAOD in Fall,

while CALIOP shows a more distinct seasonality with the highest DAOD of about 0.3 in May-

July and the lowest DAOD of <0.1 in winter. Over other PSAs in North Africa, MODIS and

CALIOP DAOD are correlated well with R^2 ≥ 0.5 in NAF-2, 3, 6 and agree well with the slope

475   close to 1 and average bias of 0.6 – 0.7 in NAF-2, 3, 4, 6 (Figure 9), and both dust retrievals

show similar seasonality (Figure 10).

In summary, MODIS and CALIOP DAOD show largest differences under the following conditions: (1) highly cloudy oceanic regions and (2) dust-pollution internal mixtures with high relative humidity. Their differences can be explained as follows.

480   1. Over cloudy ocean, cloud screening is critical to the quality of aerosol retrievals. As an active sensor, CALIOP is more reliable in discriminating clouds and aerosols than passive imager MODIS. In addition, active sensor is able to avoid impact from cloud side scattering. Therefore, MODIS is subject to more cloud contamination than CALIOP. Large cloud contamination in MODIS results in overestimation in TAOD and

485   underestimation in FMF, introducing a high bias in DAOD over ocean cloudy regions (e.g., NWP).

2. Pure dust particles are hydrophobic and will not absorb water vapor. However, for dust aerosols coated by other types of aerosols (such as the deliquescent dust-nitrate Ca(NO3)2) and saline mineral dust particles emitted from saline topsoil in arid and

490   semiarid areas (Tang et al. 2019), those types of dust particles will take up water vapor and grow to be larger in size and more spherical in shape (Wu et al. 2020). This phenomenon is most prominent for dust aerosols in polluted region (e.g., EAS) as well as with relatively high relative humidity. While such coarse spherical dust particles will not be accounted as dust in CALIOP shape-based method, they are categorized as dust in the

495   MODIS size-based method.

3.2   DAOD Inter-annual variation from CALIOP and MODIS observations

In this section we examine the inter-annual variation of DAOD captured by two sensors over some major dust source and outflow regions. Figure 11 shows a global map of DAOD

500   interannual trend derived based on the 13-year (2007-2019) time series of annual mean DAOD from CALIOP and MODIS. DAOD trend are calculated for each 2°×5° grid. Red color indicates positive trend and blue negative trend. Regions where the trend is statistically significant (p < 0.05) are marked with symbol '+'. The similar trend map for total aerosol optical depth is shown in Figure S3 in the supplementary. Overall, DAOD global pattern of interannual trend is similar

505   to TAOD in major dust-laden regions. For example, Over Sahara Desert and tropical Atlantic Ocean region, both CALIOP and MODIS do not show statistically significant trend in DAOD and TAOD. In East Asia and the northwest Pacific Ocean, both sensors show negative trend in DAOD and TAOD.

        Figure 12 displays interannual variability of annual-mean DAOD for the major dust-laden

510   regions as defined in Figure 4. Seasonal and annual DAOD trends in the nine regions are listed in Table 3. Both MODIS and CALIOP show a clear DAOD trend in certain seasons over the Eastern Asia, ARB and NWP regions. In Eastern Asia, MODIS and CALIOP show a consistent DAOD decreasing trend at a rate of $-1.7\%\ yr^{-1}$ annually. The two sensors show a DAOD decreasing tend of $-3.5\%\ yr^{-1}$ and $-2.5\%\ yr^{-1}$ respectively in Eastern Asia during spring and

515   show a consistent trend of DAOD in ARB during the fall, though with a factor of 2 difference in magnitude. In NWP, both MODIS- and CALIOP-based DAOD shows a decreasing trend of $-1.7\%\ yr^{-1}$and $-1.6\%\ yr^{-1}$, respectively. The annual DAOD decreasing trend in NWP is mainly attributed to the DAOD decline in spring at a rate of -2.3% yr^{-1} and -3.0% yr^{-1} for MODIS and CALIOP, respectively. For comparison, Shimizu et al. (2017) detect the decreasing

520   DAOD trends of $-4.3\%\ yr^{-1}$ in spring and $-2.5\%\ yr^{-1}$ on annual mean basis from the Asian Dust Network (AD-Net) lidar observations over Japan (2007-2016). These trends are greater than our results based on MODIS and CALIOP data records.

Dust over NWP comes mainly from East Asian dust sources. The broad East Asian region (ESA defined in Figure 4) show statistically significant DAOD decreasing trends (Figure 12c) which is consistent with the DAOD decreasing trend in NWP. It is also imperative to further examine which of six major PSAs in East Asia (ESA-1 to ESA-6 in Figure 7) contribute to the decreasing trend of DAOD. As shown in Figure 13, among the six PSAs, the satellite data show consistent interannual declining trend of DAOD in EAS-5 (Southern Gobi Desert) at a rate of -4.8% yr^{-1} and -2.8% yr^{-1} for MODIS and CALIOP, respectively. In spring, DAOD in EAS-5 shows a significantly declining trend at a rate of -5.6% yr^{-1} and -3.3% yr^{-1} for MODIS and CALIOP (Figure S4). Figure 14 assesses the correlation between DAOD in EAS-5 and DOAD in NWP based on MODIS and CALIOP, respectively. For annual mean DAOD from 2007 to 2019, both sensors show a good correlation between EAS-5 and NWP with $R^2 \approx 0.4$ ($p = 0.02$). In spring, the correlation of DAOD from two regions is slightly reduced based on CALIOP ($R^2 = 0.36$, $p = 0.03$), while a much weaker correlation ($R^2 = 0.28, p = 0.07$) was found based on MODIS. We further examine potential factors contribute to the declining trend of DAOD in ESA-5. The first row in Figure 15 shows the springtime trend of MODIS enhance vegetation index (EVI), MERRA2 near-surface (at 10 m) wind speed and precipitation in EAS-5 region. While EVI shows a significantly increasing trend with $R^2 = 0.71$ (p<0.05), the surface wind speed shows a decreasing trend with $R^2 = 0.36$ (p<0.05). There is no significant trend for precipitation. The second and third row in Figure 15 shows the correlations of the three factors with MODIS DAOD and CALIOP DAOD, respectively. Clearly, EVI is anti-correlated with both MODIS and CALIOP DAOD with $R^2 > 0.42$ and p<0.05. While the surface wind speed is correlated with MODIS DAOD with $R^2 = 0.53$ and p<0.05, its correlation with CALIOP DAOD is weaker ($R^2 = 0.29$ and p=0.06). Note that EVI and surface wind speed are not independent

variables that affect dust emissions. An increase of EVI or vegetation cover could reduce the surface wind speed. However, given the relatively coarse resolution of MERRA2, the surface wind speed trend may largely reflect the change in atmospheric circulations other than local wind decrease induced by more vegetation. The precipitation shows no statistically significant

550   correlation with MODIS and CALIOP DAOD.

As discussed earlier, our results suggest that the decrease of NWP DAOD is likely a result of the decreasing dust events in Asian deserts (i.e., EAS-5 Gobi) in turn likely due to change of vegetation. This is also reported in several recent studies. Sternberg et al. (2015) found that Gobi

555   Desert contracted from 2000 to 2012 due to increased moisture availability. Song et al. (2016) used an Integrated Wind Erosion Modeling System to simulate the spring dust emissions in northern China over the period of 1982 to 2011. They found a significant decrease of the magnitude of spring dust event in China which is attributed to both climate change and local mitigation strategies. Similarly, An et al., (2018) also noted a significant decrease of dust storm

560   event in East Asian after analyzing observational data from ground stations, numerical modeling, and vegetation indices obtained from both satellite and reanalysis data. Over the last few decades, Chinese government has been taking actions to restore overgrazed land in Inner Mongolia, the enlarged vegetation coverage and the expected earlier vegetation green-up due to global warming could have mitigated dust activity in this region (Fan et al. 2014). Together the results from our

565   analysis, along with the aforementioned recent studies, suggest that the decreasing springtime DAOD trend in the NWP region is a result of the decline of dust activities in the Inner Mongolia (i.e., EAS-5) which is likely linked to vegetation coverage changes in recent years as a result of China's mitigation projects to hold back desertification.

Some caveats must be mentioned, however, when interpreting the trend analysis here. First
of all, due to the limitation of satellite data record, we have only 13 years' CALIOP data and 17
years' MODIS data available. Other climate variabilities, such as the El Nino-Southern
Oscillation (ENSO), could confound the trend analysis. For example, Abish and Mohanakumar
(2013) shows that La Nina (El Nino) weakens (strengthens) the zonal circulation over the Indian
subcontinent, which result in low (high) aerosol concentration over Indian subcontinent
transported from Arabian Desert over the period. Gong et al. (2005) also shows the impact of
ENSO on the interannual variability of Asian dust loading and deposition. According to the
NOAA Oceanic Nino Index (ONI), the climate switched from a strong La Niña phase in 2010-
2011 to a strong El Niño phase in 2015-2016. However, the potential impact of ENSO on the
dust inter-annual variability is beyond the scope of this study and will be left for the future
research.

4   Uncertainty Analysis

The uncertainty of CALIOP DAOD retrieval come from several sources: One is some
technical uncertainty such as instrument calibration errors, errors in discriminating cloud from
aerosol and failure to detect aerosol layers (including tenuous aerosol layer and the lower part of
heavy dust layer. For example, Thorsen and Fu (2015) estimated that CALIOP may have
underestimated 30%-50% in the magnitude of aerosol direct radiative effect due to its low
sensitivity to tenuous layer), which is likely to translate into low bias in DAOD. In heavy aerosol
conditions (e.g., strong dust storms in source regions and outflow regions), CALIOP laser cannot
penetrate to the bottom of aerosol layer due to the laser attenuation (Chamara et al., 2017). As a
result, CALIOP AOD is biased low. DAOD is also subject to uncertainty due to the assumption

of dust lidar ratio (extinction to backscatter ratio). Different desserts produce dust with different minerology, thus different lidar ratio. Voss et al., (2001) measures LR for African dust as 41 ± 8 sr using a micropulse lidar and Liu et al. (2002) measures LR for Asian dust as 42-55 sr.

595   Globally observed lidar ratios are summarized in Müller et al., (2007) and Baars et al., (2016). Typical lidar ratio values for desert dust aerosols range from 35sr to 55sr. This study assumes dust lidar ratio to be 44 sr at 532nm, which is the value used in the CALIOP V4 product (M.-H. Kim et al. 2018) and is comparable to previous studies and nevertheless induce potential uncertainties to DAOD. When separating dust from non-dust aerosol, the choice of

600   depolarization ratio for dust aerosols and non-dust aerosols also introduces uncertainty in DAOD. To quantify the uncertainty caused by DPR selection, we also calculated DAOD in the lowest ($\delta_d = 0.30$ and $\delta_{nd} = 0.07$) and the highest ($\delta_d = 0.20$ and $\delta_{nd} = 0.02$) dust fraction scenarios. We estimated that the uncertainty in monthly DAOD is 35%-47% in regions with DAOD larger than 0.06 and up to 80% in regions with very low DAOD.

605

MODIS dust detection is also subject to some uncertainties for both over ocean and over land retrievals. Over ocean, the persistent presence of clouds in some regions (e.g., North Pacific Ocean, southeastern Atlantic Ocean) pose a challenge to MODIS aerosol retrievals, probably causing a high AOD bias, and low FMF bias, and thereby a high DAOD bias. In addition,

610   DAOD was calculated from the MODIS-retrieved AOD (τ) and FMF (f) with appropriate parameterizations of marine aerosol AOD (τ_m), FMF of dust (f_{dust}), combustion (f_c) and marine (f_m) aerosols. All the parameterizations could also introduce uncertainty in the derived DAOD, in particular on a regional basis (see details in Yu et al. 2020). Over land, the derived MODIS DAOD represents the coarse-mode fraction of dust only. The exclusion of fine mode of dust

615 aerosol at emission could induce a less than 10% underestimation of the emitted mass (Kok et al.

2017). The comparison of Aqua MODIS DAOD retrievals against AERONET coarse-mode

AOD shows that Aqua MODIS DAOD values are underestimated with an error of

0.08+0.52DAOD (Pu and Ginoux, 2018).

A rigorous way to evaluate these uncertainties and validate the two dust detection

620 methods is to compare with an independent measurement of DAOD. AERONET measurements

have been considered as ground truth and often used to evaluate satellite aerosol optical depth

retrievals. However, so far there is not a valid method to derive DAOD from AERONET AOD

measurements to compare our results with. Some studies use coarse-mode AOD from

AERONET measurements as a proxy for DAOD (Pu and Ginoux, 2018), while CALIOP-based

625 DAOD retrieval and MODIS-based oceanic DAOD retrieval do not assume dust aerosols are

exclusively coarse particles. Therefore, AERONET measurements could not be used to validate

DAOD retrievals in this study.

5 Summary and Conclusion

630 Following the methodology in Yu et al. (2015a), we extend the study in both temporal

and spatial scale to present monthly mean climatology data for dust aerosol horizontal and

vertical distributions on a global scale for the period from 2007 to 2019 based on MODIS and

CALIOP observations. Our product captures very well as much hot spots along the 'dust belt'

region well, as weaker signals in other dust active regions such as Southwestern United States,

635 Patagonian Desert in South America, Central Australia, and South Africa (Figure 1). Since

DAOD climatology product contains and mixes the information of the intensity and frequency of

dust activities, we introduce the conditional DAOD product, which diminishes impacts from dust

frequency by excluding dust-free cases in the average. The comparison between DAOD

climatology data and conditional DAOD data suggests that dust activities in those regions are

640   highly episodic. As a result, the dust events in those regions may be missed by CALIOP which

has a very limited spatial sampling coverage.

CALIOP distinguishes dust aerosols based on its non-spherical shape, whereas MODIS

separates dust aerosols from others based on its large size characteristics. The discrepancy in

dust retrieval based on two instruments are expected due to the uncertainty associated with their

645   TAOD retrieval and the uncertainty associated with their different mechanism in dust detection

and separation. The comparison between CALIOP dust retrieval and MODIS dust retrieval

facilitate a better understanding of advantages and limitations of each dust product and also

provide some insights on dust morphology and dust size. Through the comparison, we found

generally CALIOP-based DAOD correlates well with MODIS-based DAOD over dust-laden

650   regions such as Sahara, TAT, CRB and ARB, but with CALIOP-based DAOD 18%, 34%, 54%

and 31% lower than MODIS-based DAOD over those regions respectively. This result is

consistent with the different treatment of the dust-pollution mixtures in the dust separation

approaches of two instruments. The better agreement (k=0.82) and correlation (R^2=0.61) in

Sahara Desert suggest that dust aerosols are irregular non-spherical and at the same time large in

655   size in this region. In some regions such as NWP, the DAOD correlation between two sensors is

quite low. There could be many reasons for this, for example, the total TAOD retrievals from

MODIS have larger uncertainty due to cloud contamination, or the DAOD retrieval from

CALIOP may miss coarse spherical dust-pollution mixtures.

The interannual variability of DAOD over dust-laden regions show no clear trend except

660   the NWP region at a rate of $-1.6\% \, yr^{-1}$ and $-1.7\% \, yr^{-1}$ based on CALIOP and MODIS

respectively, this trend is mainly attributed to the decreasing trend in spring with a rate of $-3.0\%\ yr^{-1}$ based on CALIOP and $-2.3\%\ yr^{-1}$ based on MODIS. Further investigation of DAOD trend in six dust source areas in Eastern Asian where NWP dust aerosols come from shows that there is an obvious decreasing trend in DAOD over Southern Gobi Desert based on

665 both CALIOP and MODIS dust retrievals. The decreasing trend of DAOD is correlated significantly with the vegetation index and surface wind speed in the area, whereas there is almost no correlation with the precipitation.

Data availability. The global DAOD and dust vertical extinction coefficient climatology data

670   derived from CALIOP in this study and the MODIS DAOD retrieval data over ocean are

available at

'https://drive.google.com/drive/folders/1aQVupe7govPwR6qmsqUbR4fJQsp1DBCX?usp=shari

ng'. The MODIS DAOD retrieval data over land can be requested from Dr. Paul Ginoux. The

MODIS Enhanced Vegetation Index (EVI) data could be downloaded from

675   'https://lpdaac.usgs.gov/products/myd13c2v006/#tools'. The MERRA2 surface wind speed and

precipitation data are available at

'https://disc.sci.gsfc.nasa.gov/datasets/M2T1NXFLX_5.12.4/summary?keywords=%22MERRA-

2%22'.

680   *Acknowledgement.* Qianqian Song and Zhibo Zhang cordially acknowledge the funding support

from the Future Investigators in NASA Earth and Space Science and Technology (FINESST).

Zhibo Zhang's research is supported by NASA grant (80NSSC20K0130) from the CALIPSO

and CloudSat program. HY was supported by NASA's the Science of Terra, Aqua, and Suomi-

NPP and the CALIPSO/CloudSat Science Team programs administered by Dr. Hal Maring and

685   Dr. David Considine, respectively. The computations in this study were performed at the UMBC

High Performance Computing Facility (HPCF). The facility is supported by the US National

Science Foundation through the MRI program (grant nos. CNS-0821258 and CNS-1228778) and

the SCREMS program (grant no. DMS-0821311), with substantial support from UMBC. The

MODIS aerosol data were obtained from the NASA Level-1 and Atmosphere Archive and

690   Distribution System (LAADS) webpage (https://ladsweb.nascom.nasa.gov/). The CALIOP

aerosol products were obtained from NASA Langley Research Center Atmospheric Science Data

Center (https://eosweb.larc.nasa.gov/).

Table 1. Summary of DAOD retrievals from MODIS and CALIOP

Sensors	Retrieve Scope	Relevant variables used to derive DAOD	References
MODIS	Ocean	AOD, fine-mode AOD	Yu et al. (2009, 2020)
MODIS	Land	AOD, Spectral SSA, Angstrom exponent	Pu and Ginoux et al. (2018)
CALIOP	Globe	Profiles of backscatter, extinction, depolarization ratio	Yu et al. (2015a)

695

Table 2. Global (60° S-60° N) seasonal mean DAOD and TAOD based on MODIS and CALIOP (2007~2019) dust retrievals.

		MAM		JJA		SON		DJF		Annual	
		DAOD	TAOD	DAOD	TAOD	DAOD	TAOD	DAOD	TAOD	DAOD	TAOD
MODIS	Ocean	0.056	0.148	0.060	0.149	0.045	0.141	0.050	0.141	0.053	0.145
	Land	0.125	0.277	0.112	0.267	0.073	0.195	0.082	0.210	0.099	0.237
	Global	0.072	0.179	0.075	0.180	0.052	0.155	0.056	0.155	0.063	0.167
	Land /Ocean	2.32	1.87	1.91	1.80	1.65	1.39	1.67	1.49	1.90	1.64
CALIOP	Ocean	0.02	0.094	0.022	0.096	0.014	0.088	0.015	0.085	0.018	0.091
	Land	0.076	0.177	0.075	0.204	0.046	0.166	0.041	0.136	0.059	0.171
	Global	0.035	0.116	0.036	0.125	0.023	0.109	0.022	0.099	0.029	0.112
	Land /Ocean	3.76	1.89	3.37	2.13	3.23	1.89	2.68	1.60	3.31	1.89

700   Table 3. DAOD inter-seasonal trend over major dust-laden regions based on MODIS and CALIOP observations. The changing rate of DAOD trend is shown in a sequence of annual/spring/summer/fall/winter in each cell of the table. Those statistically meaningful trends with p<0.05 are shown in bold.

	MODIS [% yr^{-1}]					CALIOP [% yr^{-1}]				
	Annual	MAM	JJA	SON	DJF	Annual	MAM	JJA	SON	DJF
Sahara Desert (a)	-0.04	-0.84	0.21	0.29	0.51	-0.09	-0.93	0.34	-0.52	0.55
Middle East (b)	0.32	-0.61	-0.02	**1.80**	1.37	**-1.84**	-2.36	-1.86	**-2.46**	-0.09
Eastern Asia (c)	**-1.74**	**-3.48**	-0.28	-0.33	-0.56	**-1.70**	**-2.46**	**-1.99**	-0.45	-1.42
TAT (d)	0.34	-0.68	-0.03	1.68	1.32	-0.25	-1.41	-0.07	0.91	-0.09
CRB (e)	1.10	0.78	0.94	**1.59**	**1.97**	-0.40	-1.39	-0.34	0.79	-1.09
MED (f)	0.10	0.32	0.49	-0.71	0.03	-1.09	-1.07	-1.63	-1.20	-0.52
NWP (g)	**-1.67**	**-2.33**	**-1.93**	0.63	-1.35	**-1.58**	**-3.01**	**-2.89**	-0.40	-0.19
ARB (h)	-1.42	-0.72	-1.81	**-1.85**	-0.31	-1.17	-1.70	-0.46	**-3.60**	-0.06
IND (i)	-0.09	-0.51	0.40	0.38	-0.89	-1.96	-2.92	-2.43	-0.21	-0.54

705
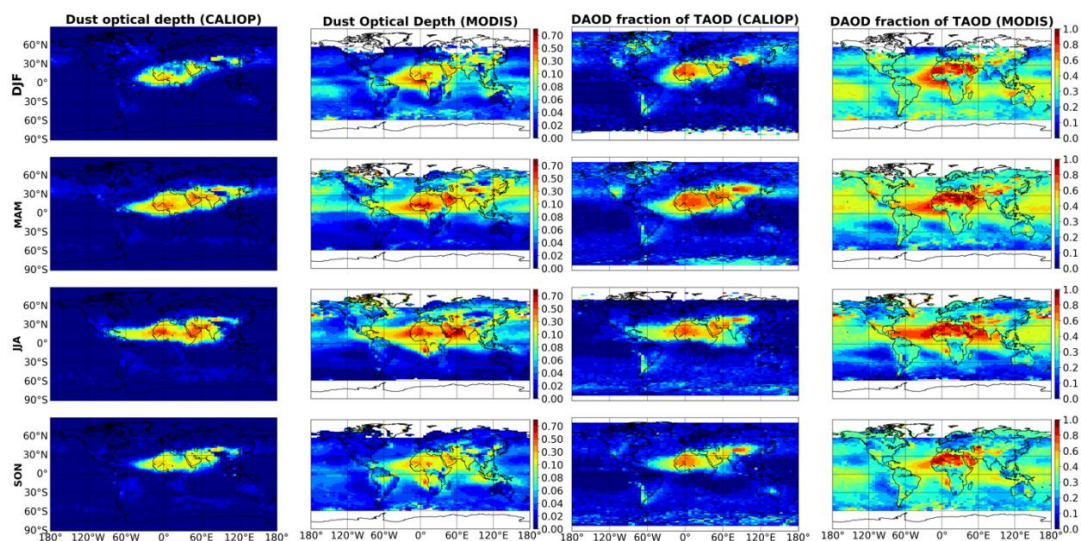
Figure 1. Spatial distribution of the seasonal mean CALIOP-based DAOD, MODIS-based DAOD and the fraction of DAOD with respect to the TAOD based on CALIOP and MODIS respectively for the globe at a $5° \ longitude \times 2° \ latitude$ resolution based on 13-year (2007-2019) CALIOP measurements.
710   **DJF**: December from previous year-January-February; **MAM**: March-April-May; **JJA**: June-July-August;
SON: September-October-November.
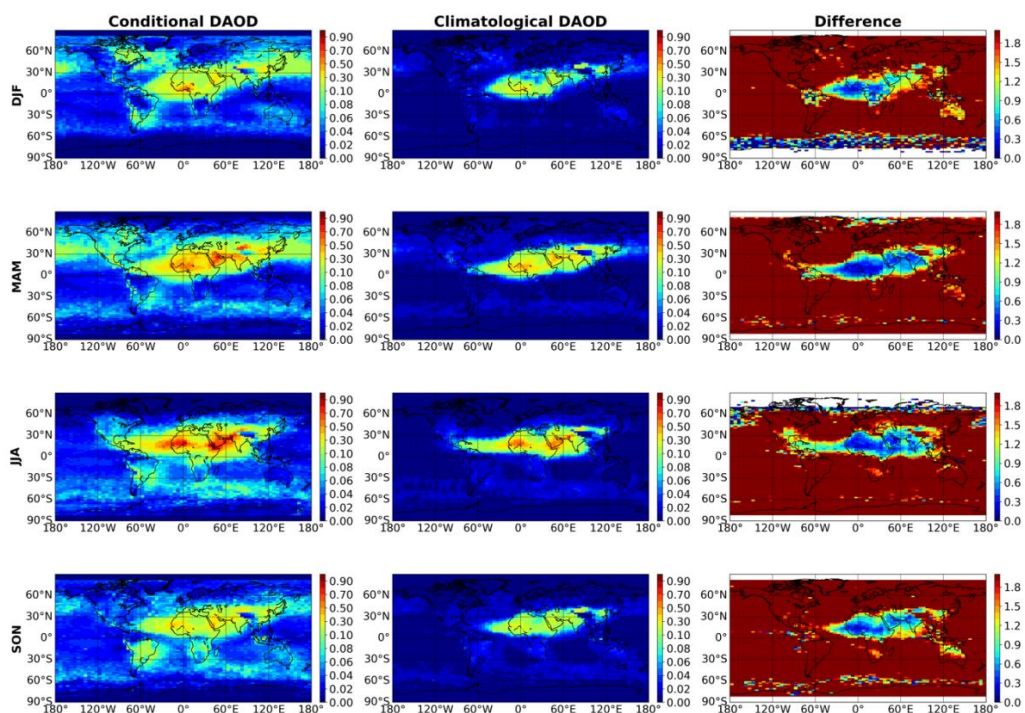
Figure 2. Conditional DAOD (the first column), climatological DAOD (the second column) based on CALIOP dust retrieval from 2007 to 2019. The third column shows the relative difference between conditionally sampled DAOD and climatological DAOD with respect to the climatological DAOD expressed in fraction.

715
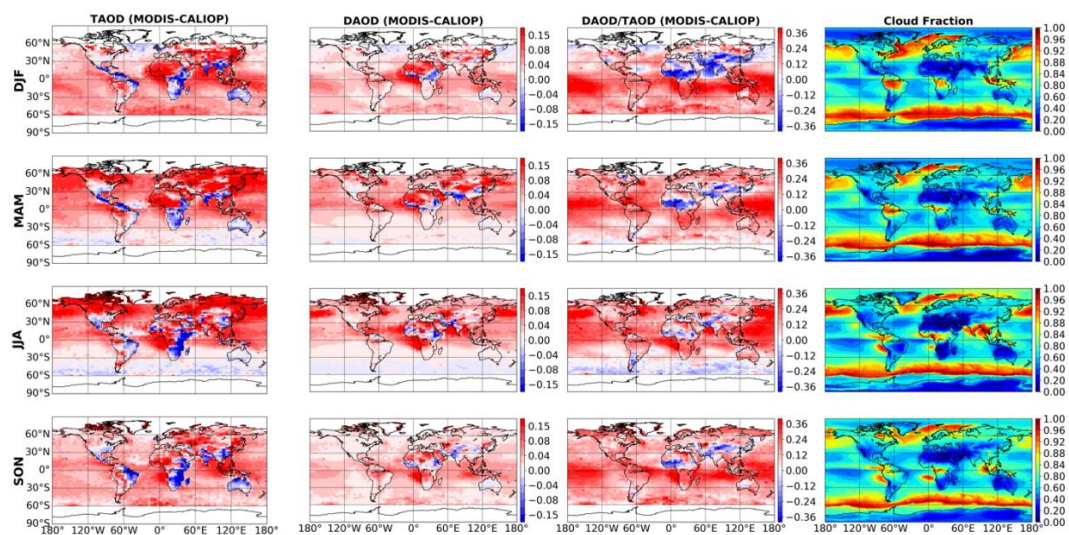
720

Figure 3. The difference between MODIS and CALIOP for seasonal mean TAOD (the first column), DAOD (the second column), and the fraction of DAOD in TAOD (the third column) on a basis of 13-year (2007-2019) average. The fourth column is the seasonal mean cloud fraction from MODIS L3 product.
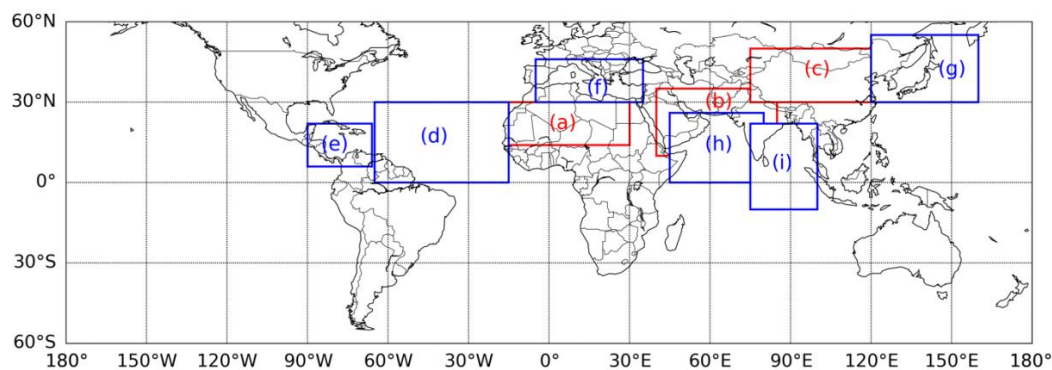
725

Figure 4. Major dust-laden regions including three dust source regions on land (a ~ c) and six outflow regions over ocean (e ~ i). (a) Sahara Desert (14ºN-30ºN, 15ºW-30ºE), (b) Middle East (10ºN-35ºN, 40ºE-85ºE) and (c) Eastern Asia (30ºN-50ºN,75ºE-130ºE) (d) the tropical Atlantic Ocean–TAT (0º-30ºN, 15ºW-60ºW), (e) the Caribbean Sea–CRB (6ºN-22ºN, 60ºW-90ºW), (f) the Mediterranean Sea–MED
730 (30ºN-46ºN, 5ºW-35ºE), (g) the northwest Pacific Ocean–NWP (30ºN-55ºN, 120ºE-160ºE), (h) the Arabian Sea–ARB (0º-26ºN,45ºE-80ºE and (i) the tropical Indian Ocean and the Bay of Bengal–IND (10ºS-22ºN,75ºE-100ºE). Note we only consider grids over land for the three dust source regions and grids over ocean for the six dust outflow regions.

735
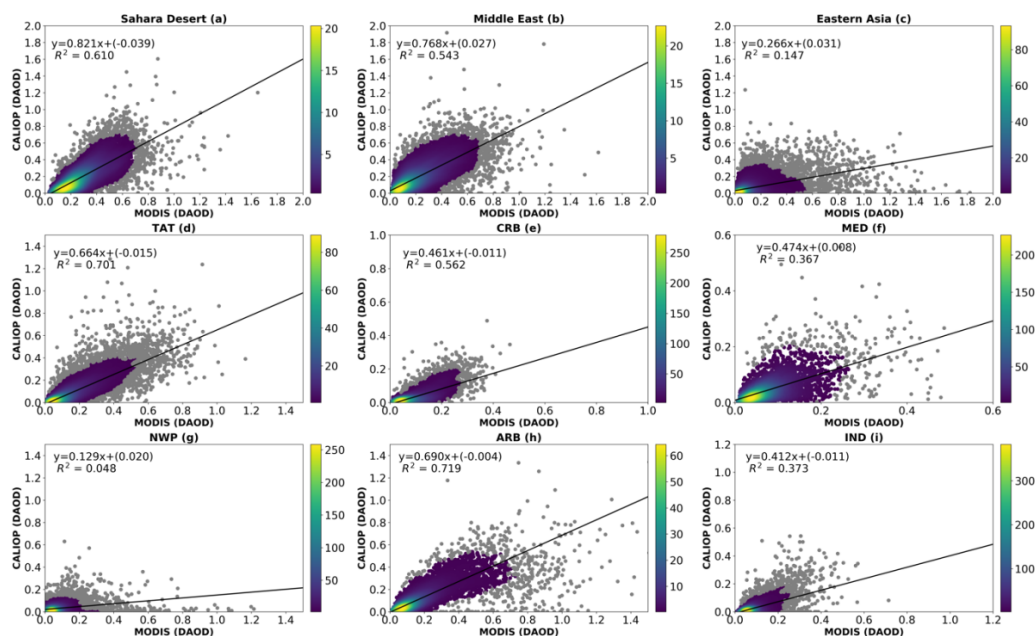
Figure 5. Comparison of CALIOP DAOD against MODIS DAOD over dust-laden regions indicated in Figure 4. Color represents the probability density using gaussian kernel density estimation. Grey points represent data points within the lowest 5% of data density. Those grey points are excluded in the linear regression analysis.

740
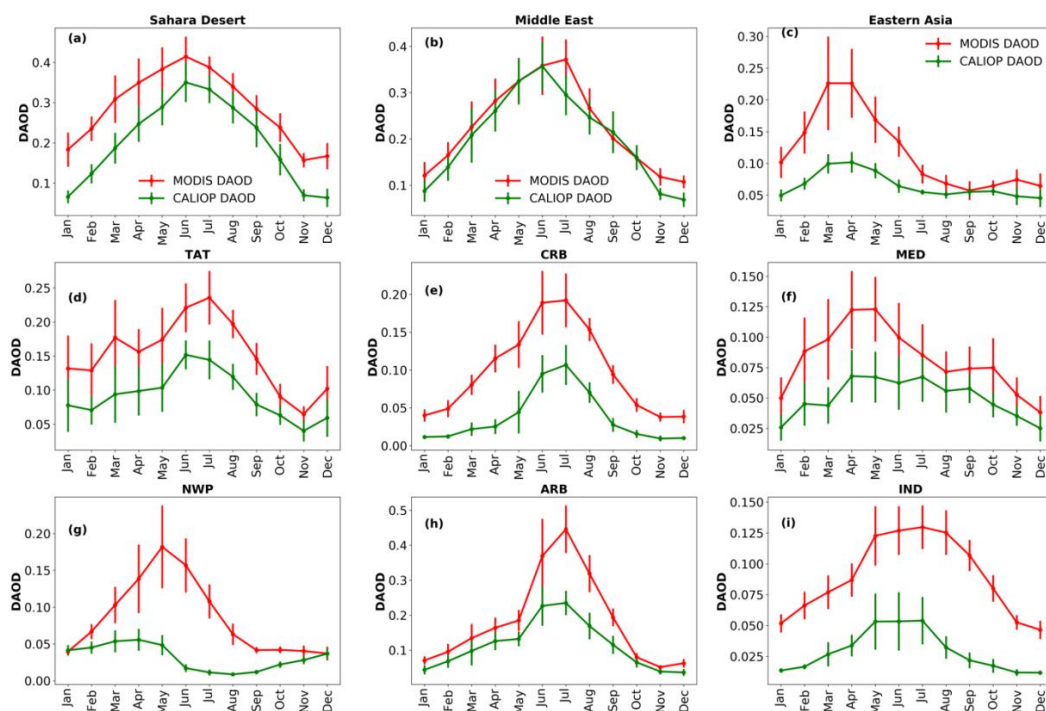
Figure 6. Monthly variation of DAOD from CALIOP (green) and MODIS (red) for major dust-laden regions indicated in Figure 4. Vertical line represents ±1 sigma (standard deviation) over the 13-year period.
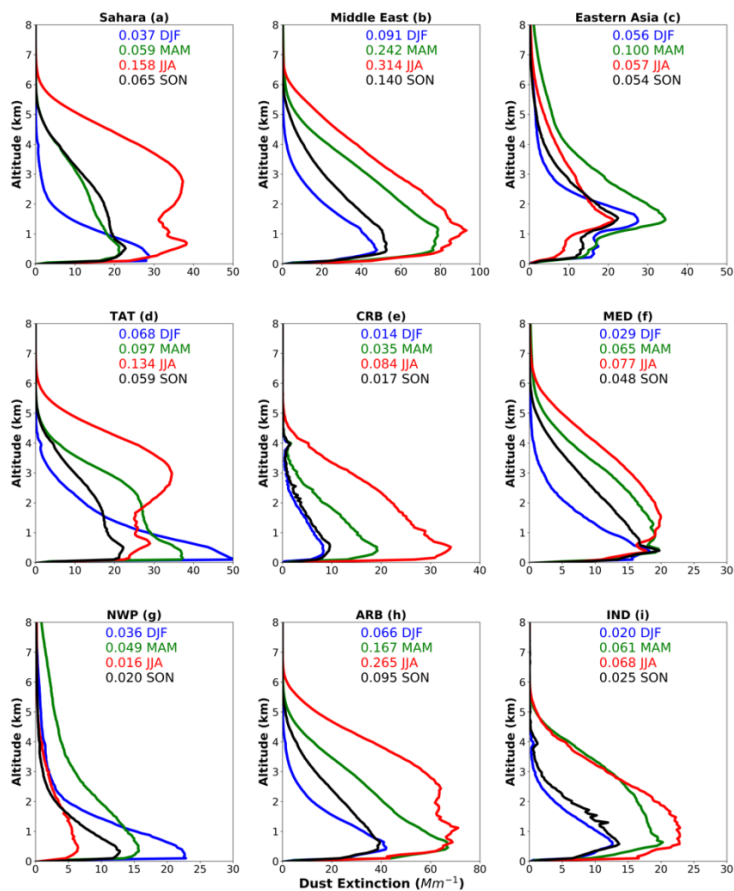
750

Figure 7. Vertical profiles of seasonal mean dust extinction coefficient (Mm^{-1}) in 9 dust-laden regions indicated in Figure 4. Different colors represent different seasons. The numbers on each plot are the seasonal mean DAOD for the region.

755
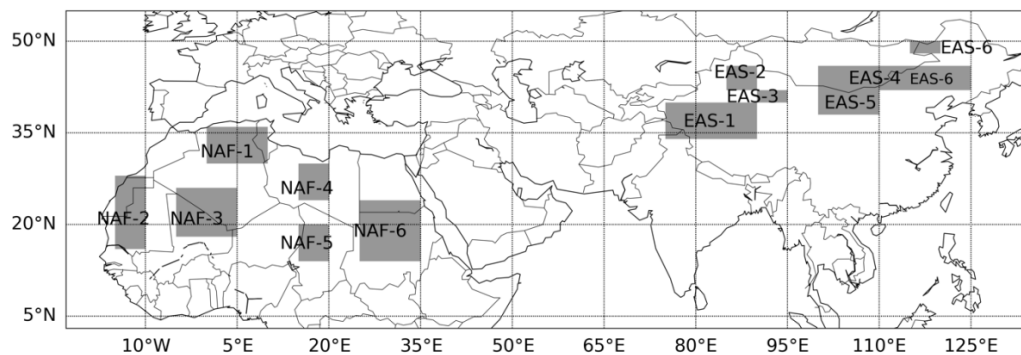
Figure 8. Six dust potential source subregions in Northern Africa (NAF) and Eastern Asia (EAS) based
on Fig.1. and Fig. 2. in Formenti, et al., 2011. PSA NAF-1(30N-36N, 0-9E), PSA NAF-2 (16N-28N,
10W-15W), PSA NAF-3 (18N-26N, 5W-5E), PSA NAF-4 (24N-30N, 15E-20E), PSA NAF-5 (14N-20N,
15E-20E), PSA NAF-6 (14N-24N, 25E-35E); EAS-1: (34N-40N, 75E-90E) ; EAS-2: (44N-46N, 85E-
90E); EAS-3: (40N-42N,90E-95E and 42N-44N, 85E-90E); EAS-4: (42N-46N, 100E-115E); EAS-5:
(38N-42N, 100E-110E); EAS-6: (42N-46N, 115E-125E and 48N-50N, 115E-120E)

760

765
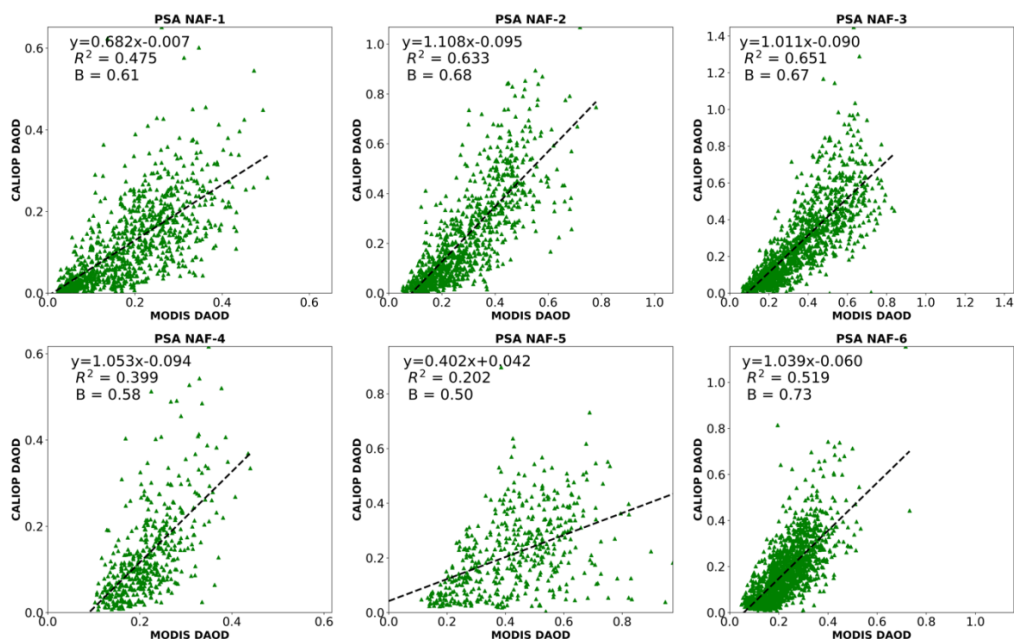
Figure 9. Comparison of CALIOP DAOD against MODIS DAOD over six dust aerosol source regions in North Africa from NAF-1 to NAF-6 as indicated in Figure 8. The mean bias (B) is computed as the average of CALIOP DAOD / MODIS DAOD ratios of all data pairs. B =1, >1, <1 indicates no bias, high bias and low bias.
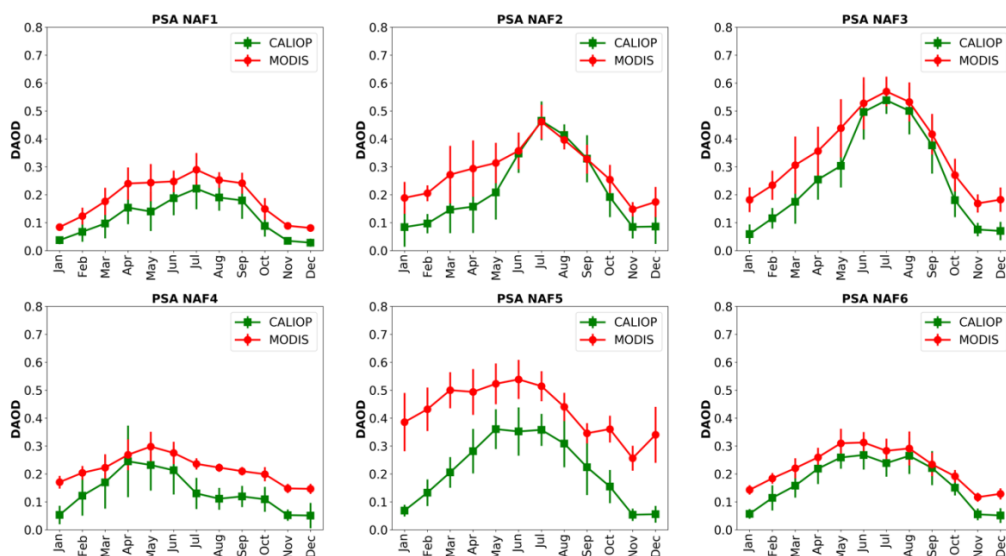
Figure 10. Annual cycle of 13-year (2007-2019) monthly mean DAOD over the six PSAs of North African dust.
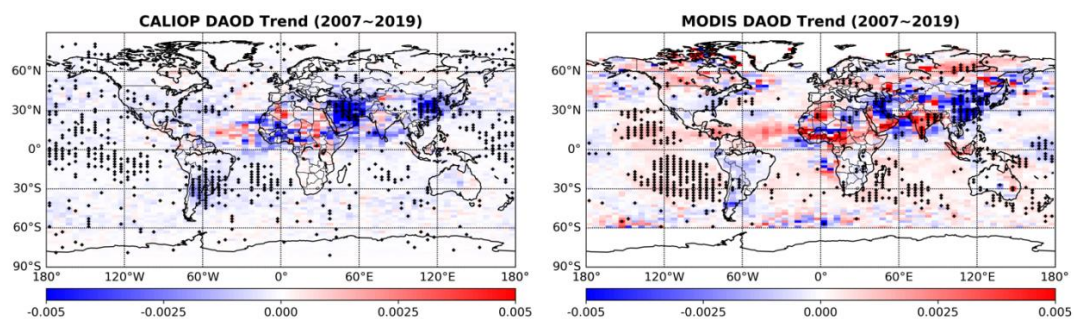
780 Figure 11. Global map of DAOD decadal trend based on CALIOP (left) and MODIS (right) dust climatology data over 2007-2019 period. Red and blue represents increasing and decreasing trend, respectively. Symbol '+' denotes trends with p-value < 0.05, which are considered as statistically meaningful trend.

785
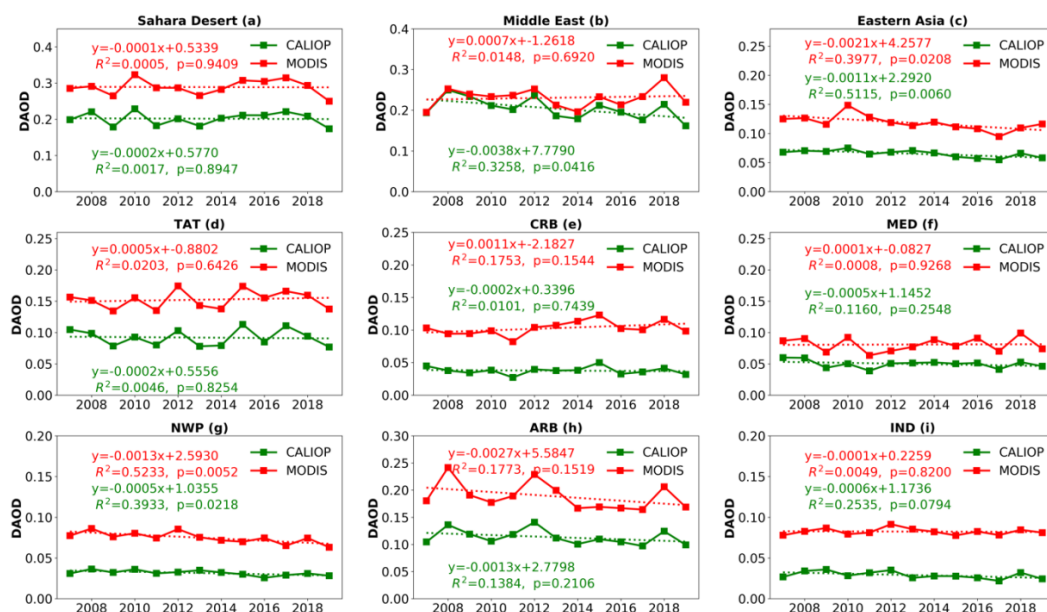
Figure 12. DAOD interannual variability over main dust source regions (a-c) and dust outflow regions (d-i) revealed by CALIOP (green curve) and MODIS (red curve) observations.

790
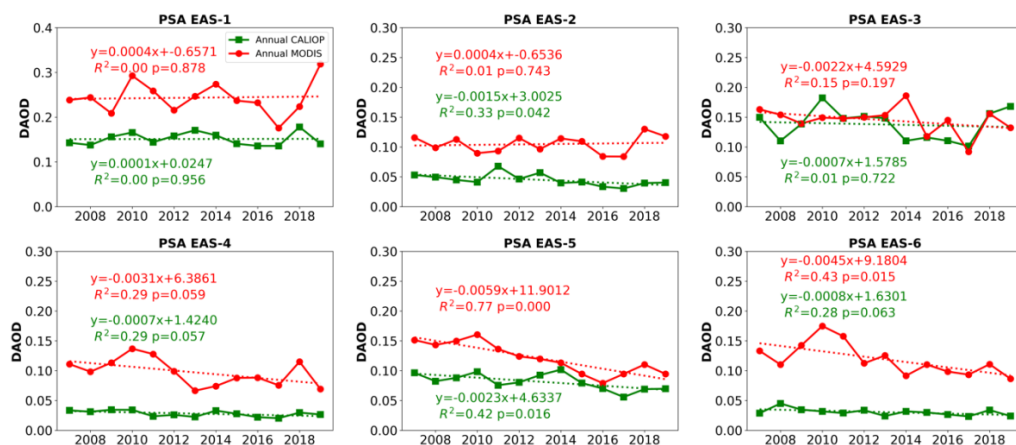
Figure 13. Interannual variability of CALIOP (green) and MODIS (red) DAOD in the six potential dust source areas in Eastern Asia (refer to Figure 8).

795
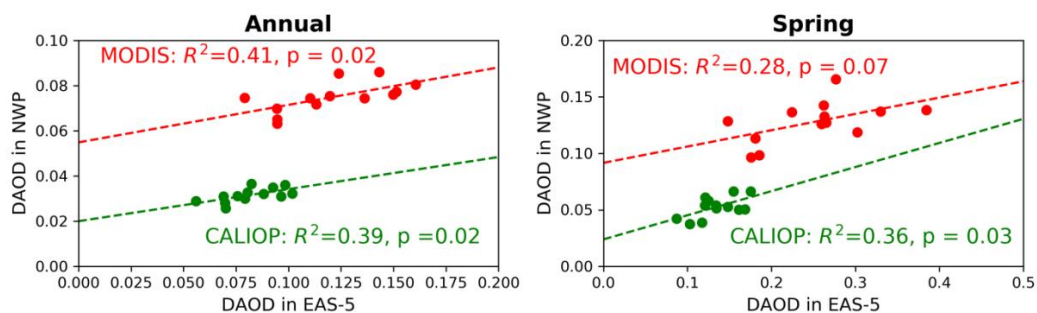
800   Figure 14. Correlation between DAOD in EAS-5 (Southern Gobi Desert) and DAOD in NWP for annual mean (left) and springtime average (right).
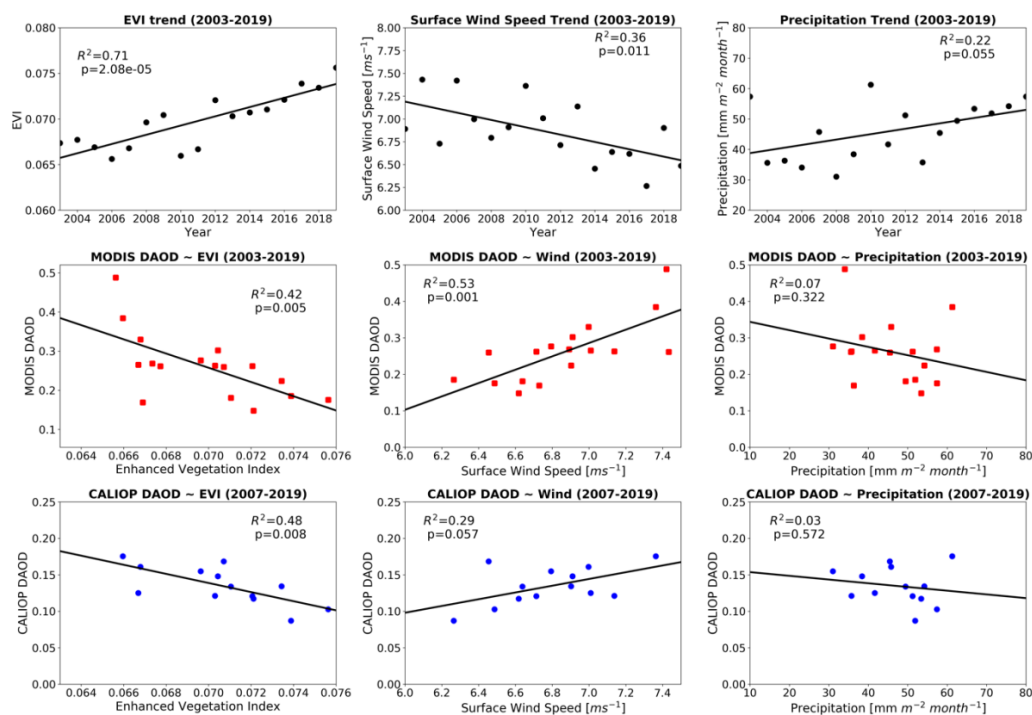
805   Figure 15. The inter-annual trend of Enhance Vegetation Index (EVI), surface wind speed and precipitation and their correlation with DAOD in spring, EAS5 region. The 1st row shows inter-annual trend of EVI, surface wind speed and precipitation. The 2nd and 3rd rows show the correlation of EVI, surface wind speed and precipitation with MODIS-based DAOD and CALIOP-based DAOD respectively.

810   References

Abish, B. and K. Mohanakumar. 2013. "Absorbing Aerosol Variability over the Indian
        Subcontinent and Its Increasing Dependence on ENSO." *Global and Planetary Change*
        106:13–19.

Ackerman, A. S., O. B. Toon, D. E. Stevens, A. J. Heymsfield, V. Ramanathan, and E. J. Welton.
815   2000. "Reduction of Tropical Cloudiness by Soot." *Science* 288(5468):1042–47.

Albrecht, B. A. 1989. "Aerosols, Cloud Microphysics, and Fractional Cloudiness." *Science*
        245(4923):1227–30.

An, Linchang, Huizheng Che, Min Xue, Tianhang Zhang, Hong Wang, Yaqiang Wang,
        Chunhong Zhou, Hujia Zhao, Ke Gui, and Yu Zheng. 2018. "Temporal and Spatial
820   Variations in Sand and Dust Storm Events in East Asia from 2007 to 2016: Relationships
        with Surface Conditions and Climate Change." *Science of The Total Environment* 633:452–
        62.

Ansmann, A., P. Seifert, Matthias Tesche, and U. Wandinger. 2012. "Profiling of Fine and
        Coarse Particle Mass: Case Studies of Saharan Dust and Eyjafjallajökull/Grimsvötn
825   Volcanic Plumes." *Atmospheric Chemistry and Physics*.

Baars, Holger, Thomas Kanitz, Ronny Engelmann, Dietrich Althausen, Birgit Heese, Mika
        Komppula, Jana Preißler, Matthias Tesche, Albert Ansmann, and Ulla Wandinger. 2016.
        "An Overview of the First Decade of PollyNET: An Emerging Network of Automated
        Raman-Polarization Lidars for Continuous Aerosol Profiling."

830   Di Biagio, C., Y. Balkanski, S. Albani, O. Boucher, and P. Formenti. 2020. "Direct Radiative
        Effect by Mineral Dust Aerosols Constrained by New Microphysical and Spectral Optical
        Data." *Geophysical Research Letters* 47(2):e2019GL086186.

Boucher, O., D. Randall, P. Artaxo, C. Bretherton, G. Feingold, P. Forster, V.-M. Kerminen, Y.
        Kondo, H. Liao, U. Lohmann, P. Rasch, S.K. Satheesh, S. Sherwood, B. Stevens and X. Y.
835   Zhang. 2013. "Clouds and Aerosols." *Climate Change 2013 The Physical Science Basis:
        Working Group I Contribution to the Fifth Assessment Report of the Intergovernmental
        Panel on Climate Change*.

Burton, S. P., R. A. Ferrare, C. A. Hostetler, J. W. Hair, R. R. Rogers, M. D. Obland, C. F.
        Butler, A. L. Cook, D. B. Harper, and K. D. Froyd. 2012. "Aerosol Classification Using
840   Airborne High Spectral Resolution Lidar Measurements-Methodology and Examples."
        Atmospheric Measurement Techniques 5(1):73.

Chen, Cheng, Oleg Dubovik, Daven K. Henze, Tatyana Lapyonak, Mian Chin, Fabrice Ducos,
        Pavel Litvinov, Xin Huang, and Lei Li. 2018. "Retrieval of Desert Dust and Carbonaceous
        Aerosol Emissions over Africa from POLDER/PARASOL Products Generated by the
845   GRASP Algorithm." *Atmospheric Chemistry and Physics* 18(16):12551–80.

Chimot, Julien, J. Pepijn Veefkind, Tim Vlemmix, Johan F. de Haan, Vassilis Amiridis,
        Emmanouil Proestakis, Eleni Marinou, and Pieternel F. Levelt. 2017. "An Exploratory
        Study on the Aerosol Height Retrieval from OMI Measurements of the 477 Nm O.Sub.2 -
        O.Sub.2 Spectral Band Using a Neural Network Approach." *Atmospheric Measurement
850   Techniques* 10:783.

Clarisse, Lieven, Cathy Clerbaux, Bruno Franco, Juliette Hadji-Lazaro, Simon Whitburn, A. K.
        Kopp, Daniel Hurtmans, and P-F Coheur. 2019. "A Decadal Data Set of Global
        Atmospheric Dust Retrieved from IASI Satellite Measurements." *Journal of Geophysical
        Research: Atmospheres* 124(3):1618–47.

855   Dubovik, O., A. Sinyuk, T. Lapyonok, B. N. Holben, M. Mishchenko, P. Yang, T. F. Eck, H.

Volten, O. Munoz, B. Veihelmann, W. J. van der Zande, J. F. Leon, M. Sorokin, and I. Slutsker. 2006. "Application of Spheroid Models to Account for Aerosol Particle Nonsphericity in Remote Sensing of Desert Dust." *Journal of Geophysical Research-Atmospheres* 111(D11).

860   Esselborn, Michael, Martin Wirth, Andreas Fix, Bernadett Weinzierl, Katharina Rasp, Matthias Tesche, and Andreas Petzold. 2009. "Spatial Distribution and Optical Properties of Saharan Dust Observed by Airborne High Spectral Resolution Lidar during SAMUM 2006." *Tellus B: Chemical and Physical Meteorology* 61(1):131–43.

Evan, A. T., J. Dunion, J. A. Foley, A. K. Heidinger, and C. S. Velden. 2006. "New Evidence for 865   a Relationship between Atlantic Tropical Cyclone Activity and African Dust Outbreaks." *Geophysical Research Letters* 33(19).

Fan, Bihang, Li Guo, Ning Li, Jin Chen, Henry Lin, Xiaoyang Zhang, Miaogen Shen, Yuhan Rao, Cong Wang, and Lei Ma. 2014. "Earlier Vegetation Green-up Has Reduced Spring Dust Storms." *Scientific Reports* 4:1–6.

870   Fiebig, Markus, Andreas Petzold, Ulla Wandinger, Manfred Wendisch, Christoph Kiemle, Armin Stifter, Martin Ebert, Tom Rother, and Ulrich Leiterer. 2002. "Optical Closure for an Aerosol Column: Method, Accuracy, and Inferable Properties Applied to a Biomass-burning Aerosol and Its Radiative Forcing." *Journal of Geophysical Research: Atmospheres* 107(D21):LAC-12.

875   Formenti, P., L. Schutz, Y. Balkanski, K. Desboeufs, M. Ebert, K. Kandler, A. Petzold, D. Scheuvens, S. Weinbruch, and D. Zhang. 2011. "Recent Progress in Understanding Physical and Chemical Properties of African and Asian Mineral Dust." *Atmospheric Chemistry and Physics* 11(16):8231–56.

Ge, J. M., J. P. Huang, C. P. Xu, Y. L. Qi, and H. Y. Liu. 2014. "Characteristics of Taklimakan 880   Dust Emission and Distribution: A Satellite and Reanalysis Field Perspective." *Journal of Geophysical Research: Atmospheres* 119(20):11,711-772,783.

Ginoux, P., M. Chin, I. Tegen, J. M. Prospero, B. Holben, O. Dubovik, and S. J. Lin. 2001. "Sources and Distributions of Dust Aerosols Simulated with the GOCART Model." *Journal of Geophysical Research-Atmospheres* 106(D17):20255–73.

885   Ginoux, Paul, Dmitri Garbuzov, and N. Christina Hsu. 2010. "Identification of Anthropogenic and Natural Dust Sources Using Moderate Resolution Imaging Spectroradiometer (MODIS) Deep Blue Level 2 Data." *Journal of Geophysical Research Atmospheres* 115(5):1–10.

Ginoux, Paul, Joseph M. Prospero, Thomas E. Gill, N. Christina Hsu, and Ming Zhao. 2012. "Global-Scale Attribution of Anthropogenic and Natural Dust Sources and Their Emission 890   Rates Based on MODIS Deep Blue Aerosol Products." *Reviews of Geophysics* 50(3).

Gkikas, Antonis, Emmanouil Proestakis, Vassilis Amiridis, Stelios Kazadzis, Enza Di Tomaso, Alexandra Tsekeri, Eleni Marinou, Nikos Hatzianastassiou, and Carlos Pérez García-Pando. 2020. "ModIs Dust AeroSol (MIDAS): A Global Fine Resolution Dust Optical Depth Dataset." *Atmospheric Measurement Techniques Discussions* 1–62.

895   Gong, S. L., X. Y. Zhang, T. L. Zhao, # X B Zhang, L. A. Barrie, I. G. Mckendry, and C. S. Zhao. 2005. *A Simulated Climatology of Asian Dust Aerosol and Its Trans-Pacific Transport. Part II: Interannual Variability and Climate Connections*.

Griffin, Dale W. 2007. "Atmospheric Movement of Microorganisms in Clouds of Desert Dust and Implications for Human Health." *Clinical Microbiology Reviews* 20(3):459 LP – 477.

900   Grousset, Francis E., Paul Ginoux, Aloys Bory, and Pierre E. Biscaye. 2003. "Case Study of a Chinese Dust Plume Reaching the French Alps." *Geophysical Research Letters* 30(6).

Hansen, J., M. Sato, and R. Ruedy. 1997. "Radiative Forcing and Climate Response." *Journal of Geophysical Research-Atmospheres* 102(D6):6831–64.

Hsu, N. C., M. J. Jeong, C. Bettenhausen, A. M. Sayer, R. Hansell, C. S. Seftor, J. Huang, and S. C. Tsay. 2013. "Enhanced Deep Blue Aerosol Retrieval Algorithm: The Second Generation." *Journal of Geophysical Research: Atmospheres* 118(16):9296–9315.

Hsu, N. Christina, Si Chee Tsay, Michael D. King, and Jay R. Herman. 2004. "Aerosol Properties over Bright-Reflecting Source Regions." *IEEE Transactions on Geoscience and Remote Sensing* 42(3):557–69.

Huang, Jianping, Patrick Minnis, Bin Chen, Zhongwei Huang, Zhaoyan Liu, Qingyun Zhao, Yuhong Yi, and J. Kirk Ayers. 2008. "Long-Range Transport and Vertical Structure of Asian Dust from CALIPSO and Surface Measurements during PACDEX." *Journal of Geophysical Research: Atmospheres* 113(D23).

Huang, Jianping, Patrick Minnis, Yuhong Yi, Qiang Tang, Xin Wang, Yongxiang Hu, Zhaoyan Liu, Kirk Ayers, Charles Trepte, and David Winker. 2007. "Summer Dust Aerosols Detected from CALIPSO over the Tibetan Plateau." *Geophysical Research Letters* 34(18).

Jickells, T. D., Z. S. An, K. K. Andersen, A. R. Baker, G. Bergametti, N. Brooks, J. J. Cao, P. W. Boyd, R. A. Duce, K. A. Hunter, H. Kawahata, N. Kubilay, J. Laroche, P. S. Liss, N. Mahowald, J. M. Prospero, A. J. Ridgwell, I. Tegen, and R. Torres. 2005. "Global Iron Connections Between Desert Dust, Ocean Biogeochemistry, and Climate." *Science* (308):67–71.

Kalashnikova, O. V, R. Kahn, I. N. Sokolik, and Wen-Hao Li. 2005. "Ability of Multiangle Remote Sensing Observations to Identify and Distinguish Mineral Dust Types: Optical Models and Retrievals of Optically Thick Plumes." *Journal of Geophysical Research: Atmospheres* 110(D18).

Kim, Dongchul, Mian Chin, Hongbin Yu, Xiaohua Pan, Huisheng Bian, Qian Tan, Ralph A. Kahn, Kostas Tsigaridis, Susanne E. Bauer, Toshihiko Takemura, Luca Pozzoli, Nicolas Bellouin, and Michael Schulz. 2019. "Asian and Trans-Pacific Dust: A Multimodel and Multiremote Sensing Observation Analysis." *Journal of Geophysical Research: Atmospheres* 124(23):13534–59.

Kim, M. H., A. H. Omar, J. L. Tackett, M. A. Vaughan, D. M. Winker, C. R. Trepte, Y. Hu, Z. Liu, L. R. Poole, M. C. Pitts, J. Kar, and B. E. Magill. 2018. "The CALIPSO Version 4 Automated Aerosol Classification and Lidar Ratio Selection Algorithm." *Atmospheric Measurement Techniques* 11(11):6107–35.

Kim, Man Hae, Ali H. Omar, Jason L. Tackett, Mark A. Vaughan, David M. Winker, Charles R. Trepte, Yongxiang Hu, Zhaoyan Liu, Lamont R. Poole, Michael C. Pitts, Jayanta Kar, and Brian E. Magill. 2018. "The CALIPSO Version 4 Automated Aerosol Classification and Lidar Ratio Selection Algorithm." *Atmospheric Measurement Techniques* 11(11):6107–35.

Kittaka, C., D. M. Winker, M. A. Vaughan, A. Omar, and L. A. Remer. 2011. "Intercomparison of Column Aerosol Optical Depths from CALIPSO and MODIS-Aqua." *Atmospheric Measurement Techniques* 4(2):131–41.

Klüser, L., D. Martynenko, and T. Holzer-Popp. 2011. "Thermal Infrared Remote Sensing of Mineral Dust over Land and Ocean: A Spectral SVD Based Retrieval Approach for IASI." *Atmospheric Measurement Techniques* 4(5):757–73.

Kok, Jasper F., David A. Ridley, Qing Zhou, Ron L. Miller, Chun Zhao, Colette L. Heald, Daniel S. Ward, Samuel Albani, and Karsten Haustein. 2017. "Smaller Desert Dust Cooling Effect Estimated from Analysis of Dust Size and Abundance." *Nature Geoscience*

10(4):274–78.

Koren, I., Y. J. Kaufman, L. A. Remer, and J. V Martins. 2004. "Measurement of the Effect of Amazon Smoke on Inhibition of Cloud Formation." *Science* 303(5662):1342–45.

Lau, K. M. and K. M. Kim. 2007. "Cooling of the Atlantic by Saharan Dust." *Geophysical Research Letters* 34(23).

Levy, Robert C., Shana Mattoo, Virginia Sawyer, Yingxi Shi, Peter R. Colarco, Alexei I. Lyapustin, Yujie Wang, and Lorraine A. Remer. 2018. "Exploring Systematic Offsets between Aerosol Products from the Two MODIS Sensors." *Atmospheric Measurement Techniques* 11(7):4073–92.

Li, W. J. and L. Y. Shao. 2009. "Observation of Nitrate Coatings on Atmospheric Mineral Dust Particles." *Atmospheric Chemistry and Physics* 9(6):1863–71.

Liu, Zhaoyan, Nobuo Sugimoto, and Toshiyuki Murayama. 2002. "Extinction-to-Backscatter Ratio of Asian Dust Observed with High-Spectral-Resolution Lidar and Raman Lidar." *Applied Optics* 41(15):2760–67.

Mbourou, G. N'Tchayi, J. J. Bertrand, and S. E. Nicholson. 1997. "The Diurnal and Seasonal Cycles of Wind-Borne Dust over Africa North of the Equator." *Journal of Applied Meteorology* 36(7):868–82.

Mielonen, T., A. Arola, M. Komppula, J. Kukkonen, J. Koskinen, G. De Leeuw, and K. E. J. Lehtinen. 2009. "Comparison of CALIOP Level 2 Aerosol Subtypes to Aerosol Types Derived from AERONET Inversion Data." *Geophysical Research Letters* 36(18).

Miller, R. L. and I. Tegen. 1998. "Climate Response to Soil Dust Aerosols." *Journal of Climate* 11(12):3247–67.

Müller, Detlef, Albert Ansmann, Ina Mattis, Matthias Tesche, Ulla Wandinger, Dietrich Althausen, and G. Pisani. 2007. "Aerosol-type-dependent Lidar Ratios Observed with Raman Lidar." *Journal of Geophysical Research: Atmospheres* 112(D16).

N'Tchayi Mbourou, G., J. J. Bertrand, and S. E. Nicholson. 1997. "The Diurnal and Seasonal Cycles of Wind-Borne Dust over Africa North of the Equator." *Journal of Applied Meteorology* 36(7):868–82.

Omar, A. H., D. M. Winker, J. L. Tackett, D. M. Giles, J. Kar, Z. Liu, M. A. Vaughan, K. A. Powell, and C. R. Trepte. 2013. "CALIOP and AERONET Aerosol Optical Depth Comparisons: One Size Fits None." *Journal of Geophysical Research Atmospheres* 118(10):4748–66.

Omar, Ali H., David M. Winker, Chieko Kittaka, Mark A. Vaughan, Zhaoyan Liu, Yongxiang Hu, Charles R. Trepte, Raymond R. Rogers, Richard A. Ferrare, Kam Pui Lee, Ralph E. Kuehn, and Chris A. Hostetler. 2009. "The CALIPSO Automated Aerosol Classification and Lidar Ratio Selection Algorithm." *Journal of Atmospheric and Oceanic Technology* 26(10):1994–2014.

Parrington, Josef R., WILLIAM H. ZOLLER, and NAMIK K. ARAS. 1983. "Asian Dust: Seasonal Transport to the Hawaiian Islands." *Science* 220(4593):195 LP – 197.

Proestakis, Emmanouil, Vassilis Amiridis, Eleni Marinou, Aristeidis K. Georgoulias, Stavros Solomos, Stelios Kazadzis, Julien Chimot, Huizheng Che, Georgia Alexandri, Ioannis Binietoglou, Vasiliki Daskalopoulou, Konstantinos A. Kourtidis, Gerrit De Leeuw, and Ronald J. Van Der A. 2018. "Nine-Year Spatial and Temporal Evolution of Desert Dust Aerosols over South and East Asia as Revealed by CALIOP." *Atmospheric Chemistry and Physics* 18(2):1337–62.

Prospero, Joseph M. 1999. "Long-Range Transport of Mineral Dust in the Global Atmosphere:

Impact of African Dust on the Environment of the Southeastern United States."
995   *Proceedings of the National Academy of Sciences of the United States of America*
       96(7):3396–3403.

Prospero, Joseph M., Paul Ginoux, Omar Torres, Sharon E. Nicholson, and Thomas E. Gill. 2002.
       "Environmental Characterization of Global Sources of Atmospheric Soil Dust Identified
       with the Nimbus 7 Total Ozone Mapping Spectrometer (TOMS) Absorbing Aerosol
1000   Product." *Reviews of Geophysics* 40(1):2-1-2–31.

Pu, Bing and Paul Ginoux. 2018. "How Reliable Are CMIP5 Models in Simulating Dust Optical
       Depth?" *Atmospheric Chemistry and Physics* 18(16):12491–510.

Querol, Xavier, Aurelio Tobías, Noemí Pérez, A. Karanasiou, Fulvio Amato, Massimo Stafoggia,
       C. Pérez García-Pando, P. Ginoux, Francesco Forastiere, and Sophie Gumy. 2019.
1005   "Monitoring the Impact of Desert Dust Outbreaks for Air Quality for Health Studies."
       Environment International 130:104867.

Rajapakshe, Chamara, Zhibo Zhang, John E. Yorks, Hongbin Yu, Qian Tan, Kerry Meyer,
       Steven Platnick, and David M. Winker. 2017. "Seasonally Transported Aerosol Layers over
       Southeast Atlantic Are Closer to Underlying Clouds than Previously Reported."
1010   *Geophysical Research Letters* 44(11):5818–25.

Remer, L. A., Y. J. Kaufman, D. Tanre, S. Mattoo, D. A. Chu, J. V Martins, R. R. Li, C. Ichoku,
       R. C. Levy, R. G. Kleidman, T. F. Eck, E. Vermote, and B. N. Holben. 2005. "The MODIS
       Aerosol Algorithm, Products, and Validation." *Journal of the Atmospheric Sciences*
       62(4):947–73.

1015   Rosenfeld, D. and I. M. Lensky. 1998. "Satellite-Based Insights into Precipitation Formation
       Processes in Continental and Maritime Convective Clouds." *Bulletin of the American
       Meteorological Society* 79(11):2457–76.

Sakai, Tetsu, Tomohiro Nagai, Yuji Zaizen, and Yuzo Mano. 2010. "Backscattering Linear
       Depolarization Ratio Measurements of Mineral, Sea-Salt, and Ammonium Sulfate Particles
1020   Simulated in a Laboratory Chamber." *Applied Optics* 49(23):4441–49.

Schuster, G. L., M. Vaughan, D. MacDonnell, W. Su, D. Winker, O. Dubovik, T. Lapyonok, and
       C. Trepte. 2012. "Comparison of CALIPSO Aerosol Optical Depth Retrievals to
       AERONET Measurements, and a Climatology for the Lidar Ratio of Dust." *Atmospheric
       Chemistry and Physics* 12(16):7431–52.

1025   Shao, Y. P., K. H. Wyrwoll, A. Chappell, J. P. Huang, Z. H. Lin, G. H. McTainsh, M. Mikami, T.
       Y. Tanaka, X. L. Wang, and S. Yoon. 2011. "Dust Cycle: An Emerging Core Theme in
       Earth System Science." *Aeolian Research* 2(4):181–204.

Shimizu, Atsushi, Nobuo Sugimoto, Tomoaki Nishizawa, Yoshitaka Jin, and Dashdondog
       Batdorj. 2017. "Variations of Dust Extinction Coefficient Estimated by Lidar Observations
1030   over Japan, 2007-2016." *Scientific Online Letters on the Atmosphere* 13:205–8.

Song, Hongquan, Kesheng Zhang, Shilong Piao, and Shiqiang Wan. 2016. "Spatial and
       Temporal Variations of Spring Dust Emissions in Northern China over the Last 30 Years."
       Atmospheric Environment 126:117–27.

Song, Q., Z. Zhang, H. Yu, S. Kato, P. Yang, P. Colarco, L. A. Remer, and C. L. Ryder. 2018.
1035   "Net Radiative Effects of Dust in the Tropical North Atlantic Based on Integrated Satellite
       Observations and in Situ Measurements." *Atmospheric Chemistry and Physics* 18(15).

Sternberg, Troy, Henri Rueff, and Nick Middleton. 2015. "Contraction of the Gobi Desert, 2000-
       2012." *Remote Sensing* 7(2):1346–58.

Su, L. and O. B. Toon. 2011. "Saharan and Asian Dust: Similarities and Differences Determined

1040   by CALIPSO, AERONET, and a Coupled Climate-Aerosol Microphysical Model."
    Atmospheric Chemistry and Physics 11(7):3263–80.

  Tang, Mingjin, Huanhuan Zhang, Wenjun Gu, Jie Gao, Xing Jian, Guoliang Shi, Bingqi Zhu,
    Luhua Xie, Liya Guo, Xiaoyan Gao, Zhe Wang, Guohua Zhang, and Xinming Wang. 2019.
    "Hygroscopic Properties of Saline Mineral Dust From Different Regions in China:
1045   Geographical Variations, Compositional Dependence, and Atmospheric Implications."
    Journal of Geophysical Research: Atmospheres 124(20):10844–57.

  Textor, C., M. Schulz, S. Guibert, S. Kinne, Y. Balkanski, S. Bauer, T. Berntsen, T. Berglen, O.
    Boucher, M. Chin, F. Dentener, T. Diehl, R. Easter, H. Feichter, D. Fillmore, S. Ghan, P.
    Ginoux, S. Gong, A. Grini, J. Hendricks, L. Horowitz, P. Huang, I. Isaksen, T. Iversen, S.
1050   Kloster, D. Koch, A. Kirkevåg, J. E. Kristjansson, M. Krol, A. Lauer, J. F. Lamarque, X.
    Liu, V. Montanaro, G. Myhre, J. Penner, G. Pitari, S. Reddy, Ø. Seland, P. Stier, T.
    Takemura, and X. Tie. 2006. *Analysis and Quantification of the Diversities of Aerosol Life
    Cycles within AeroCom*. Vol. 6.

  Thorsen, Tyler J. and Qiang Fu. 2015. "CALIPSO-Inferred Aerosol Direct Radiative Effects:
1055   Bias Estimates Using Ground-Based Raman Lidars." *Journal of Geophysical Research*
    120(23):12,209-12,220.

  Twomey, Sean. 1977. "The Influence of Pollution on the Shortwave Albedo of Clouds." *Journal
    of the Atmospheric Sciences* 34(7):1149–52.

  Uno, Itsushi, Kenta Eguchi, Keiya Yumimoto, Toshihiko Takemura, Atsushi Shimizu, Mitsuo
1060   Uematsu, Zhaoyan Liu, Zifa Wang, Yukari Hara, and Nobuo Sugimoto. 2009. "Asian Dust
    Transported One Full Circuit around Theglobe." *Nature Geoscience* 2(8):557–60.

  Voss, Kara K. and Amato T. Evan. 2020. "A New Satellite-Based Global Climatology of Dust
    Aerosol Optical Depth." *Journal of Applied Meteorology and Climatology* 59(1):83–102.

  Voss, Kenneth J., Ellsworth J. Welton, Patricia K. Quinn, James Johnson, Anne M. Thompson,
1065   and Howard R. Gordon. 2001. "Lidar Measurements during Aerosols99." *Journal of
    Geophysical Research: Atmospheres* 106(D18):20821–31.

  Winker, D. M., J. L. Tackett, B. J. Getzewich, Z. Liu, M. A. Vaughan, and R. R. Rogers. 2013.
    "The Global 3-D Distribution of Tropospheric Aerosols as Characterized by CALIOP."
    Atmospheric Chemistry and Physics 13:3345.

1070  Winker, David M., Mark A. Vaughan, Ali Omar, Yongxiang Hu, Kathleen A. Powell, Zhaoyan
    Liu, William H. Hunt, and Stuart A. Young. 2009. "Overview of the CALIPSO Mission and
    CALIOP Data Processing Algorithms." *Journal of Atmospheric and Oceanic Technology*
    26(11):2310–23.

  Wu, Tong, Zhanqing Li, Jun Chen, Yuying Wang, Hao Wu, Xiao'ai Jin, Chen Liang, Shangze Li,
1075   Wei Wang, and Maureen Cribb. 2020. "Hygroscopicity of Different Types of Aerosol
    Particles: Case Studies Using Multi-Instrument Data in Megacity Beijing, China." *Remote
    Sensing* 12(5).

  Xu, Hui, Fengjie Zheng, and Wenhao Zhang. 2016. "Variability in Dust Observed over China
    Using A-Train Caliop Instrument." *Advances in Meteorology* 2016(2015).

1080  Yang, W., A. Marshak, O. V Kalashnikova, and A. B. Kostinski. 2012. "CALIPSO Observations
    of Transatlantic Dust: Vertical Stratification and Effect of Clouds." *Atmospheric Chemistry
    and Physics* 12:11339.

  Yorks, J. E., S. P. Palm, D. L. Hlavka, M. J. McGill, E. Nowottnick, P. Selmer, and W. D. Hart.
    2015. "The Cloud-Aerosol Transport System (CATS) Algorithm Theoretical Basis
1085   Document."

Young, Stuart A., Mark A. Vaughan, Anne Garnier, Jason L. Tackett, James D. Lambeth, and Kathleen A. Powell. 2018. "Extinction and Optical Depth Retrievals for CALIPSO's Version 4 Data Release." *Atmospheric Measurement Techniques* 11:5701.

Yu, H. B., M. Chin, H. S. Bian, T. L. Yuan, J. M. Prospero, A. H. Omar, L. A. Remer, D. M. Winker, Y. K. Yang, Y. Zhang, and Z. B. Zhang. 2015 (a). "Quantification of Trans-Atlantic Dust Transport from Seven-Year (2007-2013) Record of CALIPSO Lidar Measurements." *Remote Sensing of Environment* 159:232–49.

Yu, H. B., M. Chin, T. L. Yuan, H. S. Bian, L. A. Remer, J. M. Prospero, A. Omar, D. Winker, Y. K. Yang, Y. Zhang, Z. B. Zhang, and C. Zhao. 2015 (b). "The Fertilizing Role of African Dust in the Amazon Rainforest: A First Multiyear Assessment Based on Data from Cloud-Aerosol Lidar and Infrared Pathfinder Satellite Observations." *Geophysical Research Letters* 42(6):1984–91.

Yu, Hongbin, Mian Chin, Lorraine A. Remer, Richard G. Kleidman, Nicolas Bellouin, Huisheng Bian, and Thomas Diehl. 2009. "Variability of Marine Aerosol Fine-Mode Fraction and Estimates of Anthropogenic Aerosol Component over Cloud-Free Oceans from the Moderate Resolution Imaging Spectroradiometer (MODIS)." *Journal of Geophysical Research Atmospheres* 114(10):1–11.

Yu, Hongbin, Mian Chin, David M. Winker, Ali H. Omar, Zhaoyan Liu, Chieko Kittaka, and Thomas Diehl. 2010. "Global View of Aerosol Vertical Distributions from CALIPSO Lidar Measurements and GOCART Simulations: Regional and Seasonal Variations." *Journal of Geophysical Research Atmospheres* 115(4):1–19.

Yu, Hongbin, Lorraine A. Remer, Mian Chin, Huisheng Bian, Qian Tan, Tianle Yuan, and Yan Zhang. 2012. "Aerosols from Overseas Rival Domestic Emissions over North America." *Science* 337(6094):566–69.

Yu, Hongbin, Lorraine A. Remer, Ralph A. Kahn, Mian Chin, and Yan Zhang. 2013. "Satellite Perspective of Aerosol Intercontinental Transport: From Qualitative Tracking to Quantitative Characterization." *Atmospheric Research* 124:73–100.

Yu, Hongbin, Qian Tan, Mian Chin, Lorraine A. Remer, Ralph A. Kahn, Huisheng Bian, Dongchul Kim, Zhibo Zhang, Tianle Yuan, Ali H. Omar, David M. Winker, Robert C. Levy, Olga Kalashnikova, Laurent Crepeau, Virginie Capelle, and Alain Chédin. 2019. "Estimates of African Dust Deposition Along the Trans-Atlantic Transit Using the Decadelong Record of Aerosol Measurements from CALIOP, MODIS, MISR, and IASI." *Journal of Geophysical Research: Atmospheres* 124(14):7975–96.

Yu, Hongbin, Yang Yang, Hailong Wang, Qian Tan, Mian Chin, Robert Levy, Lorraine Remer, Steven Smith, Tianle Yuan, and Yingxi Shi. 2020. "Interannual Variability and Trends of Combustion Aerosol and Dust in Major Continental Outflows Revealed by MODIS Retrievals and CAM5 Simulations During 2003–2017." *Atmospheric Chemistry and Physics Discussions* 1–38.

Yu, Yan, Olga V Kalashnikova, Michael J. Garay, and Michael Notaro. 2019. "Climatology of Asian Dust Activation and Transport Potential Based on MISR Satellite Observations and Trajectory Analysis." *Atmospheric Chemistry & Physics* 19(1).